Rapid Estimation of Activation Enthalpies for Cytochrome-P450-Mediated Hydroxylations

ARTHUR N. MAYENO,[1,2] JONATHAN L. ROBINSON,[1,2] BRAD REISFELD[1,2,3]
[1]*Systems and Computational Biology Research Group, Colorado State University, Fort Collins, Colorado 80523*
[2]*Department of Chemical and Biological Engineering, Colorado State University, Fort Collins, Colorado 80523*
[3]*Department of Environmental and Radiological Health Sciences, Colorado State University, Fort Collins, Colorado 80523*

Received 7 April 2010; Revised 25 June 2010; Accepted 11 July 2010
DOI 10.1002/jcc.21649
Published online 5 October 2010 in Wiley Online Library (wileyonlinelibrary.com).

Abstract: Cytochrome P450 (CYP) enzymes play a critical role in detoxication and bioactivation of xenobiotics; thus, the ability to predict the biotransformation rates and regioselectivity of CYP enzymes toward substrates is an important goal in toxicology and pharmacology. Here, we present the use of the semiempirical quantum chemistry method SAM1 to rapidly estimate relative activation enthalpies ($\Delta H^{\ddagger}$) for the hydroxylation of aliphatic carbon centers of various substrates. The $\Delta H^{\ddagger}$ were determined via a reaction path calculation, in the reverse direction (RRP), using the iron-hydroxo-porphine intermediate and the substrate radical. The SAM1 $\Delta H^{\ddagger}$ were calculated via unrestricted Hartree-Fock (UHF) and configuration interaction (CI) formalisms for both the doublet and quartet spin states. The SAM1 RRP $\Delta H^{\ddagger}$, after subtracting a correction factor, were compared with density functional theory (DFT) B3LYP activation energies for two sets of substrates and showed R^2 ranging from 0.69 to 0.89, and mean absolute differences ranging from 1.2 $\pm$ 1.0 to 1.7 $\pm$ 1.5 kcal/mol. SAM1 UHF and CI RRP calculation times were, on average, more than 200 times faster than those for the corresponding forward reaction path DFT calculations. Certain key transition-state (TS) geometry measurements, such as the forming O···H bond length, showed good correlation with the DFT values. These results suggest that the SAM1 RRP approach can be used to rapidly estimate the DFT activation energy and some key TS geometry measurements and can potentially be applied to estimate substrate hydroxylation rates and regioselectivity by CYP enzymes.

 J Comput Chem 32: 639–657, 2011

Key words: prediction; cytochrome P450; activation energy; hydrogen abstraction; semiempirical

Introduction

Rapid methods to predict the rate and regioselectivity of xenobiotic biotransformations by cytochrome P450 (CYP) enzymes would be useful in medicine, toxicology, as well as in the pharmaceutical and chemical industries, because of the importance of metabolism in pharmacokinetics, detoxication, and bioactivation.[1–3] Development of *in silico* approaches to predict CYP metabolism has been the subject of intense research for a number of decades, especially in recent years as computational methods have improved in speed and accuracy.[4–28] Software packages and tools to predict biotransformation, using various approaches, are available and include CypScore,[26] EaMEAD,[27] MetaDrug,[11] MetaSite,[9] Meteor,[10] and others.[4–8,12–25,28]

Traditionally, determination of biotransformation has been accomplished through *in vitro* and *in vivo* experimentation. Although advancements in high throughput technologies have dramatically reduced the cost and time of *in vitro* experiments, the ability to predict biotransformation *in silico* is highly desirable for many reasons, including, *inter alia*, the cost and speed to prescreen potential new drug candidates or reexamine extant chemicals whose toxicology has not been examined thoroughly. Attempts to predict rates and regioselectivity of CYP reactions, however, have been difficult, because of multiple confounding factors, including the promiscuity (broad substrate specificity)[29] of CYP enzymes toward

Additional Supporting Information may be found in the online version of this article.

The content is solely the responsibility of the authors and does not necessarily represent the official views of NIEHS or the National Institutes of Health.

Correspondence to: A. N. Mayeno; e-mail: arthur.mayeno@colostate.edu

Contract/grant sponsor: National Institute of Environmental Health Sciences (NIEHS); contract/grant number: K25ES012909

substrates, the existence of multiple CYP isoforms and their allelic variants (polymorphism),[30] the allosteric behavior[31–34] of some CYP isozymes, the difficulty in obtaining 3D (crystal) structures of the isozymes until recently,[35] the possible presence of multiple forms of the active oxygen species within CYP (e.g., iron-oxo, hydroperoxy-iron, and peroxo-iron),[36–38] and its spin multiplicity (high and low spin states).[39–41] The general consensus is that accurate prediction of biotransformation by individual CYP isozymes requires consideration of both the intrinsic reactivity of each site within the substrate and the contribution of the CYP active site in orienting the substrate relative to the active oxygenating species.[12]

The active oxygenating species that can be used to rationalize most CYP-generated metabolites is the porphyrin-iron-oxo form, called compound I (Cpd I), and also denoted as "FeO^{3+}."[42] Transition-state geometries and energies of some substrates and Cpd I have been calculated using density functional theory (DFT)[21,39,40] and wavefunction approaches,[43–45] but a drawback of these methodologies is the calculation time and the exacting procedures required to locate a transition state or states. Semiempirical methods using simple surrogates (e.g., *p*-nitrosophenoxy and methoxy radicals) for Cpd I have also been studied,[12,46–49] but their predictive ability for substrates outside the sets used in developing the models is uncertain.

Hydroxylation, a major biotransformation carried out by CYP enzymes, is associated with both detoxication and bioactivation (e.g., the solvent chloroform, chemotherapy drug cyclophosphamide, and organophophorus insecticides).[1,2] Here, we examine the use of the semiempirical method, semi-*ab initio* model 1 (SAM1),[50–52] with a more realistic model of Cpd I (abbreviated OFeSX, where X = H or CH_3; Fig. 1 shows the nonoxygenated structure) to provide a rapid method to estimate activation enthalpies for hydroxylation by CYP enzymes. Activation enthalpies can be related to reaction rates and regioselectivity (when the activation enthalpies are calculated for each intramolecular site).[53] SAM1-calculated activation enthalpies for hydroxylation reactions by Cpd I showed good correlation with those determined by DFT methods, based on 21 substrates (24 sites) studied by Olsen et al.[12] and 10 substrates (11 sites) by Shaik et al.[21] TS geometries calculated by SAM1 were also compared with those obtained by DFT, and certain key geometry measurements, such as the forming O···H bond length, showed good correlation with the DFT values.

Computational Methods

Computational Tools

Semiempirical SAM1 quantum mechanical calculations were performed using AMPAC 9.1.3 (Semichem, Shawnee Mission, KS) with Agui 9.1.3 (GUI; Semichem, Shawnee Mission, KS); in addition, DFT calculations were performed using Gaussian 03 (G03),[54] version 6.1 for Windows (Gaussian, Wallingford, CT), with GaussView 4.1[55] (Semichem, Shawnee Mission, KS), on a Dell Precision workstation, with two quad core Intel® Xeon® Processors, X5460, 3.16 GHz, and 8 GB RAM (3 GB usable with Windows XP, 32-bit), or a compute cluster comprising six Dell 2950 servers linked via a SMC gigabit switch, with each server running CentOS (v5.2) Linux and containing two quad-core 2.5 GHz Xeon® processors, 8 GB RAM, and a 146 GB hard drive; the cluster contains 3 TB additional hard disk space (RAID 5) made available to all nodes via NFS.

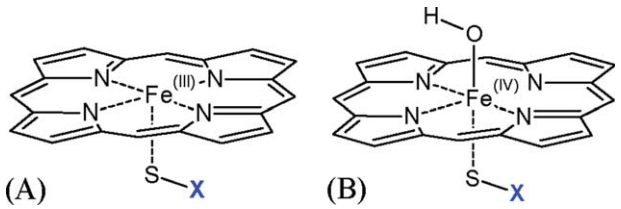

Figure 1. (A) Simplified model used for heme and the proximal ligand, where X = H or CH_3. (B) Iron-hydroxo-porphine (HOFeSX) used for the reverse reaction path (RRP) approach. [Color figure can be viewed in the online issue, which is available at wileyonlinelibrary.com.]

Geometry Optimization

The TS calculation approach was similar to that previously reported.[49] For additional computational details, see Supporting Information. All calculations were for the gas phase. Each SAM1 TS structure was verified by the presence of only one imaginary frequency and by an intrinsic reaction coordinate calculation, whereas all stable geometries were verified by the absence of imaginary frequencies. The unrestricted Hartree-Fock (UHF) and restricted HF (RHF) formalism were used for open-shell and closed-shell systems, respectively, unless an alternative method (e.g., configuration interaction, CI) is indicated. Specific issues regarding calculations are described in the sections below. SAM1 spin density data for OFeSX, HOFeSX, as well as for the TSs are listed in Supporting Information Table S1.

Reaction Path Calculations

Reverse reaction path (RRP) (coordinate) calculations were performed using SAM1 as follows, unless otherwise noted. (a) The substrate radical and HOFeSX (Fig. 1B) were optimized separately. (b) The optimized substrate radical was placed so that the reacting carbon center was exactly 2 Å from the hydrogen of HOFeSX, and the orientation adjusted so that the O—H···C bond angle was ~160° (bent away from the porphine ring). The substrate radical orientation was then manually adjusted to maximize, through visual inspection, the distance between the other atoms of the substrate radical and the porphine ring (to minimize steric interaction). (c) The distance between the radical center and H (of HOFeSX) was decreased from exactly 2 to 1 Å, in 75 evenly spaced steps of 0.0133 Å. And, (d) The heat of formation of the transition state, H_f(TS), was obtained from the highest point in the reaction path. The activation enthalpy ($\Delta H^{\ddagger}$) was calculated by subtracting the H_f of the reactants (OFeSX and substrate; individually optimized) from H_f(TS), unless otherwise noted. For these substrates, the starting orientation of the substrate radical relative to HOFeSX generally had a negligible effect on the TS geometry attained, except for two substrates: propane(2) and ethylbenzene(1), where the number in parentheses indicates the carbon from which the hydrogen is abstracted. In each of these cases, the alternate TS structure had the substrate rotated 180° from the other (see Supporting Information Fig. S1). In AMPAC, the geometry at each step is optimized; thus, the AMPAC reaction path calculation is similar to the "relaxed" potential energy surface scan calculation in G03.

Configuration Interaction

For CI calculations, various CI settings were evaluated. Initially, calculations were performed using the AMPAC keyword "OPEN(1,1)"; however, all optimization calculations involving $OFeSCH_3$ gave convergence problems (see Supporting Information). AMPAC applies the "half-electron"[56] method for RHF open-shell SCF calculations, and "OPEN(*n,m*)" indicates that the *m* open [not doubly occupied] molecular orbitals (MOs) have an equal occupancy of (*n*/*m*), where *n* is the number of open-shell electrons. It was found that "OPEN(3,3)" CI calculations greatly improved the ease of optimizations, especially for the quartet spin state. The three CI-active MOs selected were the HOMO (highest occupied MO), LUMO (lowest unoccupied MO), and HOMO-1, with three CI-active MOs, the minimum number of active MOs required for a quartet calculation. For OFeSH, nearly all variations of the CI calculation settings successfully led to energy-optimized structures; however, for $OFeSCH_3$, CI optimization converged only when using three CI-active MOs (3CI) with OPEN(3,3) (see Supporting Information Fig. S2 for specific settings). To maintain consistency across calculations, 3CI OPEN(3,3) was used as the CI method for all energy optimizations of the OFeSX structures.

DFT Calculations

DFT results obtained from the literature are clearly denoted in the text, tables, and figures. For our DFT calculations, the specific calculation procedures are described in the table legends. The thermal correction to enthalpy at 298.15 K was calculated to facilitate comparison of the DFT enthalpy with that calculated using AMPAC, which is parameterized to experimental H_f at 298 K.[56] G03 default convergence criteria were used, unless otherwise noted.

Terminology and Statistical Analyses

In the text, values are given as the mean ± standard deviation, unless otherwise noted (e.g., mean ± range indicates that 2 values were averaged). "Mean absolute difference" (MAD) refers to the average of the unsigned pairwise differences. "3CI" indicates that three CI-active MOs were used in the CI calculation. When a substrate name is followed by a number in parentheses, the number indicates the carbon from which the hydrogen is abstracted. Here, the term "reaction path" is synonymous with "reaction coordinate." To facilitate easier distinction between the enthalpy of activation ($\Delta H^{\ddagger}$) and the enthalpy of formation (ΔH_f), we have omitted the leading delta from the latter and use H_f. Statistical analyses of regression models were performed using R (v. 2.10.1) (www.r-project.org).

Results and Discussion

Iron-Oxo-Porphine Models OFeSH vs. $OFeSCH_3$

Rationale for Use of OFeSH vs. $OFeSCH_3$

In computational studies, to save calculation time, the iron porphyrin IX prosthetic group is often modeled using a truncated system without the side chains, and a variety of simplified sulfur ligands to represent the cysteinate axial ligand in the CYP enzymes.[40] Thus, porphine, the simplest porphyrin, is usually used with either the sulfhydryl (HS^-) or methyl sulfide (CH_3S^-) group (Fig. 1A). Previous researchers have reported that the simpler HS^- ligand gives an ordering of electronic states more similar to the cysteinate, while the CH_3S^- ligand is more similar to the cysteinate sterically and in terms of ionization energy.[40,57] DFT computational studies of CYP reactions often examine Cpd I in two different electronic spin states, the doublet (low spin) and quartet (high spin), as both have been computed to be nearly identical (degenerate) in energy for ground-state Cpd I.[40,58,59] Thus, we examined both ligands and spin states to evaluate their effect on TS structures and energies. Göller and Clark[60] had earlier reported on SAM1 UHF energies and geometries of the various $FeSCH_3$ species in the CYP reaction cycle.

Comparison of the SAM1 Iron-Oxo-Porphine Structures (OFeSH vs. $OFeSCH_3$)

The SAM1 UHF-optimized (H_f minimized) geometries of OFeSH and $OFeSCH_3$, in the doublet spin state, were nearly identical, both displaying a similar puckering of the porphine ring (Fig. 2 and Supporting Information Fig. S3). Key bond lengths (Fe—O and Fe—S) were within 1% of each other (Table 1), although the Fe—S—X bond angle and the N—Fe—S—X dihedral angle showed larger differences: 110.9° vs. 119.3° and 17.3° vs. 24.4° for the HS^- vs. CH_3S^- ligands, respectively. The calculated H_f were also similar: 75.7 kcal/mol (OFeSH) and 80.1 kcal/mol ($OFeSCH_3$) (Table 1).

The quartet spin state, however, for both OFeSH and $OFeSCH_3$ was more difficult to optimize using SAM1 UHF, although stable structures were eventually obtained, and their geometries displayed some noteworthy differences (see Fig. 2): the O—Fe—S atoms of OFeSH exhibited a smaller bond angle (157.2°) compared to that found for $OFeSCH_3$ (173.5°) (Table 1), with the latter angle comparable to that observed for the doublet structures of OFeSH and $OFeSCH_3$. The quartet H_f of OFeSH and $OFeSCH_3$ were 94.9 and 90.4 kcal/mol, respectively (Table 1), higher than their corresponding doublets, with their relative order reversed. Thus, although the DFT B3LYP doublet–quartet energy gap is infinitesimal for OFeSH, SAM1 UHF calculations yielded a much larger energy gap of 19.2 and 10.3 kcal/mol for OFeSH and $OFeSCH_3$, respectively. The enthalpies and geometries of our SAM1-optimized $OFeSCH_3$ structures (UHF, doublet and quartet) were either identical or within 1% of those reported by Göller and Clark.[60]

The use of SAM1 CI methodology greatly facilitated the ease of the optimizations, especially for the quartet spin state, and improved the geometry (see Fig. 3): the porphine was less puckered, more in accord with DFT geometries.[21] CI enthalpies of formation (H_f) were all greater than their respective UHF values, by an average of 31.6 ± 5.1 kcal/mol (Table 1). The spin state noticeably affected the H_f: the H_f of the quartet was greater than that of the doublet by 20.7 ± 0.1(range) kcal/mol. Thus, CI showed a very large doublet–quartet energy gap for OFeSX, unlike DFT. Changing the ligand from HS^- to CH_3S^- increased H_f by an average of 4.7 ± 0.1 kcal/mol (Table 1). The SAM1 CI geometries, on the other hand, showed little dependence on

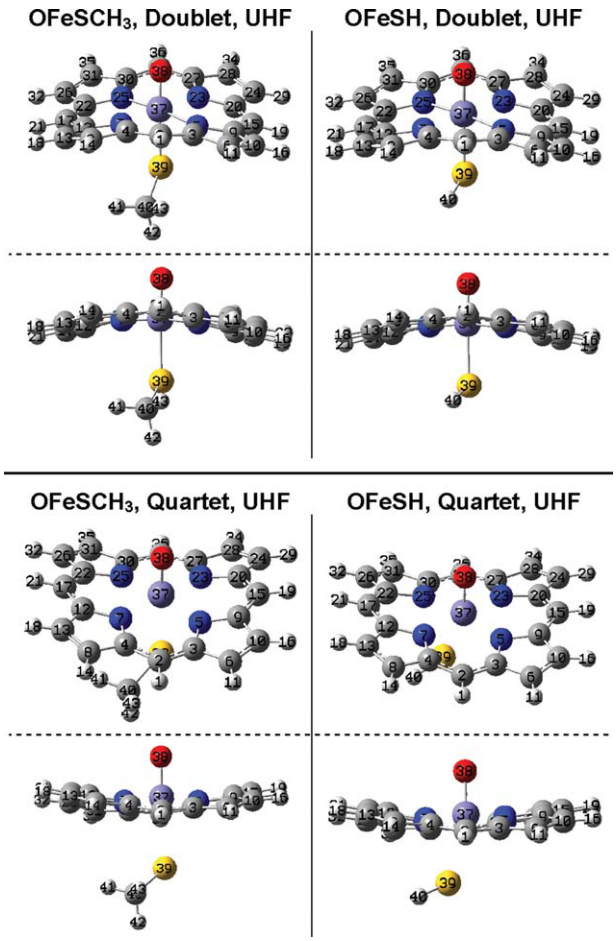

Figure 2. SAM1 UHF geometries of iron-oxo species, $OFeSCH_3$ and OFeSH. Top panel: doublet. Bottom panel: quartet. The atom numbers define geometries listed in Table 1.

the spin state, and only a slight dependence on the ligand, with the only noteworthy differences being the S—X bond distance (increase of 0.49 ± 0.00 Å changing from $OFeSCH_3$ to OFeSH) and the Fe—S—X bond angle (increase of 8.6° ± 0.3° [range] changing from $OFeSCH_3$ to OFeSH).

Comparison of the SAM1 Iron-Hydroxo-Porphine Structures HOFeSH and $HOFeSCH_3$

The iron-hydroxo-porphine (HOFeSX; X = H or CH_3), the proposed species formed after abstraction of a hydrogen atom from the substrate, was geometry optimized using SAM1 UHF. Unlike the iron-oxo-porphine species, SAM1 UHF optimization of HOFeSX was relatively facile. Singlet HOFeSH and $HOFeSCH_3$ displayed nearly identical geometries, with the minor differences limited to the dihedral angles involving the hydroxyl group: N → Fe—O—H and H—O—(Fe)—S—X (Table 2; Fig. 4 and Supporting Information Fig. S4). H_f of HOFeSH and $HOFeSCH_3$, both in their singlet states, was 82.2 and 86.0 kcal/mol, respectively. For triplet HOFeSH and $HOFeSCH_3$, the SAM1 UHF geometries were also nearly identical to each other, and very similar to those of the singlet spin state, although a larger difference for the dihedral angles (N → Fe—O—H and H—O—(Fe)—S—X) was observed between the triplets. H_f of triplet HOFeSH and $HOFeSCH_3$ was 78.4 and 82.5 kcal/mol, respectively; thus, the triplet energies were lower than the singlet energies, consistent with DFT results (Table 2). The average SAM1 UHF triplet–singlet energy gap was 3.7 ± 0.2 (range) kcal/mol, and replacing the HS^- ligand by CH_3S^- increased the energy by a mean of 4.0 ± 0.2 (range) kcal/mol. In comparison, the DFT B3LYP triplet–singlet energy gap was 14.1 and 12.6 kcal/mol for HOFeSH and $HOFeSCH_3$, respectively (Table 2).

Comparison of the SAM1 and DFT Geometries of HOFeSH and $HOFeSCH_3$

As mentioned above, the SAM1 UHF geometries for both HOFeSH and $HOFeSCH_3$ showed puckering of the porphine ring, whereas SAM1 CI geometries revealed a more planar porphine ring, similar to the DFT geometries[21] (Fig. 3 and Table 2). SAM1 UHF and CI bond lengths were generally shorter than their respective DFT B3LYP/6-31G results, with some bond distances essentially comparable (r_{SX} and r_{OH}), while others were

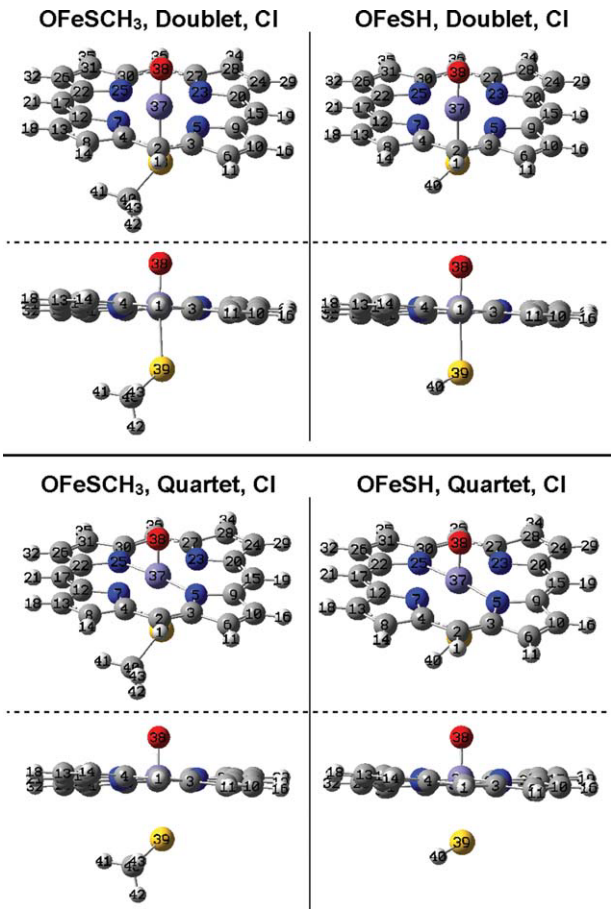

Figure 3. SAM1 CI geometries of iron-oxo species, $OFeSCH_3$ and OFeSH. Top panel: doublet. Bottom panel: quartet. AMPAC CI settings: "OPEN(3,3)." The atom numbers define geometries listed in Table 1.

Table 1. Enthalpy and Geometries of Iron-Oxo-Porphine (OFeSX), Where X = H or CH_3, Calculated by (A) SAM1 UHF and CI, and (B) DFT.

Calc type	Spin	Ligand		H_f (kcal/mol)	r_{FeO}[a]	r_{FeS}[b]	r_{SX}[c]	a_{OFeS}[d]	a_{CFeC}[e]	a_{FeSX}[f]	d_{NFeSX}[g]
SAM1 UHF	Doublet	CH_3S^-		80.05	1.49	2.30	1.84	175.3	162.8	119.3	24.4
		HS^-		75.71	1.48	2.29	1.35	176.8	162.4	110.9	17.3
	Quartet	CH_3S^-		90.37	1.55	2.74	1.79	173.5	161.5	117.1	2.9
		HS^-		94.87	1.55	2.65	1.36	157.2	162.3	109.3	2.5
SAM1 3CI active MO, OPEN(3,3)	Doublet	CH_3S^-		108.84	1.50	2.30	1.84	174.8	177.5	118.5	0.0
		HS^-		104.21	1.50	2.29	1.36	177.2	177.2	109.7	0.0
	Quartet	CH_3S^-		129.62	1.50	2.32	1.84	174.2	177.0	117.7	0.0
		HS^-		124.87	1.50	2.31	1.35	176.8	179.2	109.3	0.0
			Energy[h]	Enthalpy[i]							
DFT B3LYP	Doublet	CH_3S^-	−1625.466577	−1625.122915	1.65	2.65	1.88	170.6	176.9	109.3	13.5
		HS^-	−1586.141205	−1585.830063	1.65	2.60	1.38	171.2	174.9	98.5	26.9
	Quartet	CH_3S^-	−1625.466402	−1625.122743	1.65	2.65	1.88	171.7	174.4	109.6	15.3
		HS^-	−1586.141182	−1585.830031	1.65	2.58	1.38	173.1	175.0	98.5	26.6

AMPAC CI settings: "OPEN(3,3)." For SAM1, H_f in kcal/mol; for DFT, energy and enthalpy in hartrees. For more complete AMPAC settings, see Computational Methods and Supporting Information.
[a]Length of Fe—O bond (Å). [Atoms 37–38 in Figs. 2 and 3].
[b]Length of Fe—S bond (Å). [Atoms 37–39 in Figs. 2 and 3].
[c]Length of S—X bond (Å), where X = H for the HS^- ligand and X = C for the CH_3S^- ligand. [Atoms 39–40 in Figs. 2 and 3].
[d]O—Fe—S bond angle (°). [Atoms 38–37–39 in Figs. 2 and 3].
[e]C—Fe—C bond angle (°), a measure of the porphine ring's "pucker." [Atoms 17–37–15 in Figs. 2 and 3].
[f]Fe—S—X bond angle (°). [Atoms 37-39-40 in Figs. 2 and 3].
[g]N—Fe—S—X dihedral angle (°). [Atoms 7-37-39-40 in Figs. 2 and 3].
[h]Energy (raw) calculated at the UB3LYP/BS2//UB3LYP/BS1 level, where BS2 (basis set 2) was triple-ζ quality LACV3P+ basis set on iron and 6-311++G(2d,2p) on other atoms, whereas BS1 (basis set 1) was LACVP basis set on iron and a 6-31G basis set on other atoms.
[i]Thermal corrected enthalpy = Energy [UB3LYP/BS2] + thermal correction to enthalpy [UB3LYP/BS1 (temp = 298.15 K, pressure = 1.0 atm)]. See Supporting Information Table S20 for DFT ZPE.

more disparate ($r_{FeS,triplet}$ and r_{FeO}) (Tables 1 and 2). SAM1 CI bond angles (a_{OFeS} and a_{CFeC}) showed good agreement with the DFT values.

SAM1 UHF Transition States

Comparison with DFT TS Energies

Transition-state determination of [substrate···H···OFeSX] complexes, using DFT and wave function methods, require considerable computational cost and effort. These results are typically used to calculate activation energies to predict biotransformation rates, assess TS geometries, and gain insights into the mechanism of CYP-mediated reactions. Hydroxylation of aliphatic substrates by CYP is believed to proceed via the "oxygen rebound" mechanism proposed by Groves,[61] where $(FeO)^{3+}$ abstracts a hydrogen atom in the first step to yield $(FeOH)^{3+}$ and substrate radical, followed by recombination of hydroxyl radical from $(FeOH)^{3+}$ to give the hydroxylated substrate. As recombination has been theoretically verified to be fast, albeit influenced by spin state,[62] the relative rates of hydroxylation are dependent on the activation energy of this initial abstraction step, suggesting that prediction models based on this step are reasonable. Olsen et al.[12] had calculated DFT B3LYP activation energies for 21 substrates in the quartet spin state, whereas Shaik et al.[21] had done so for 10 substrates, in both the doublet and quartet spin states. Because Olsen et al.[12] and Shaik et al.[21] used $-SCH_3$ and $-SH$, respectively, as the proximal ligand, as well as different basis sets, their results are not directly comparable; however, within each work, the model chemistry was the same for all substrates. A study using a nonheme iron-oxo for hydrogen atom abstraction found that the more electron-donating the axial ligand is, the more reactive the iron-oxo species becomes in hydrogen atom abstraction.[63] Here, we explored the use of SAM1 for TS determination, assessing the computational cost, effort, and accuracy, relative to the DFT results of Olsen et al.[12] and Shaik et al.[21]

For the doublet spin state, the ease of determining the SAM1 UHF-optimized TS varied widely, depending on the substrate, but a valid structure was found in all cases using the reaction coordinate or substrate modification method (i.e., using a previously calculated TS and replacing atoms to give a new substrate). However, SAM1 UHF TS determination of the quartet spin state was much more difficult, and TS structures for only 11 of the 21 substrates were determined, even after exhaustive attempts (see Supporting Information Table S2 and Figs. S5 and S6). Quartet TS optimization difficulty was associated with specific substrate classes: namely, TS determination was not successful for all vinyl, carbonyl, aromatic, and amine substrates but was achievable for alkane, *O*-substituted, sulfide, and halide substrates. Thus, all substrates with a pi-system adjacent to the

Table 2. Enthalpy and Geometries of Iron-Hydroxo-Porphine (HOFeSX), Where X = H or CH_3, Calculated by (A) SAM1 UHF, and (B) DFT.

Calc type	Spin	Ligand		H_f	r_{FeO}[a]	r_{FeS}[b]	r_{SX}[c]	r_{OH}[d]	a_{OFeS}[e]	a_{CFeC}[f]	a_{FeSX}[g]	a_{FeOH}[h]	d_{NFeSX}[i]	d_{NFeOH}[j]	d_{HOSX}[k]
SAM1 UHF	Singlet	CH_3S^-		86.00	1.69	2.26	1.85	0.97	175.3	169.8	118.6	119.3	6.9	180.0	170.5
		HS^-		82.24	1.68	2.26	1.36	0.97	176.8	168.4	110.1	119.7	2.8	178.6	174.1
	Triplet	CH_3S^-		82.52	1.70	2.28	1.85	0.96	176.3	167.6	117.6	121.9	21.3	133.3	112.4
		HS^-		78.37	1.70	2.27	1.36	0.96	177.9	167.1	109.4	122.6	11.0	43.2	54.7
			Energy[l]	Enthalpy[m]											
DFT B3LYP	Singlet	CH_3S^-	−1626.098847	−1625.743844	1.81	2.29	1.88	0.98	159.7	178.4	109.9	110.5	21.6	30.6	9.8
		HS^-	−1586.775527	−1586.452623	1.81	2.30	1.38	0.98	159.8	178.2	99.0	110.5	34.6	154.4	165.2
	triplet	CH_3S^-	−1626.118460	−1625.763916	1.80	2.41	1.88	0.98	172.3	177.5	109.4	111.3	22.2	106.3	83.8
		HS^-	−1586.797515	−1586.475096	1.81	2.35	1.38	0.98	177.6	179.0	98.2	113.5	0.3	92.0	92.2

For SAM1, H_f in kcal/mol; for DFT, energy and enthalpy in hartrees. For more complete AMPAC settings, see Computational Methods and Supporting Information.

[a]Length of Fe—O bond (Å). [Atoms 37–38 in Fig. 4].

[b]Length of Fe—S bond (Å). [Atoms 37–39 in Fig. 4].

[c]Length of S—X bond (Å), where X = H for the HS^- ligand and X = C for the CH_3S^- ligand. [Atoms 39–40 in Fig. 4].

[d]Length of O—H bond (Å). [Atoms 38–44 (41 for HOFeSH) in Fig. 4].

[e]O—Fe—S bond angle (°). [Atoms 38–37–39 in Fig. 4].

[f]C—Fe—C bond angle (°), a measure of the porphine ring's 'pucker.' [Atoms 17–37–15 in Fig. 4].

[g]Fe—S—X bond angle (°). [Atoms 37–39–40 in Fig. 4].

[h]Fe—O—H bond angle (°). [Atoms 37–38–44(41) in Fig. 4].

[i]N—Fe—S—X dihedral angle (°). [Atoms 7–37–39–40 in Fig. 4].

[j]N—Fe—O—H dihedral angle (°). [Atoms 7–37–38–44(41) in Fig. 4].

[k]H—O—S—X dihedral angle (°). [Atoms 44(41)–38–39–40 in Fig. 4].

[l]Energy (raw) calculated at the UB3LYP/BS2//UB3LYP/BS1 level, where BS2 (basis set 2) was triple-ζ quality LACV3P+ basis set on iron and 6-311++G(2d,2p) on other atoms, whereas BS1 (basis set 1) was LACVP basis set on iron and a 6-31G basis set on other atoms.

[m]Thermal corrected enthalpy = Energy [UB3LYP/BS2] + thermal correction to enthalpy [UB3LYP/BS1 (temp = 298.15 K, pressure = 1.0 atm)]. See Supporting Information Table S20 for DFT ZPE.

reactive carbon center failed to optimize to a valid TS when in the quartet spin state.

A linear regression of UHF SAM1 doublet $\Delta H^{\ddagger}$, using $OFeSCH_3$, against the DFT quartet activation energies calculated by Olsen et al.[12] showed a coefficient of determination (R^2) of 0.76 (see Fig. 5). The SAM1 doublet energies were compared to DFT quartet energies because of the inability to calculate the SAM1 quartet TS for all substrates. All SAM1 $\Delta H^{\ddagger}$ were notably greater than their corresponding DFT activation energies, by an average difference of 24.7 ± 2.5 kcal/mol (Table 3). When this value is subtracted from the SAM1 $\Delta H^{\ddagger}$, the mean absolute difference (MAD) from DFT results was 1.7 ± 1.8 kcal/mol (Table 3 and Fig. 6).

After offset, the substrate with the greatest [SAM1 − DFT] $\Delta H^{\ddagger}$ difference was methane (Δ = 7.7 kcal/mol), followed by fluoroethane(1) (−4.4 kcal/mol), isopropylbenzene (−3.8 kcal/mol), and prop-1-en-2-ol (3.4 kcal/mol). No clear structural features were identified that were associated with the deviation, although $\Delta H^{\ddagger}$ of some substrates, with a double bond located α to the reacting carbon, was overestimated by SAM1 UHF relative to DFT, whereas the presence of fluorine on the reactive carbon resulted in underestimation by SAM1 UHF. Aromatic substrates also tended to be underestimated by SAM1 UHF. For the TS structures of the sulfur-containing substrates, the sulfur atom showed interaction with a carbon of the porphine ring (Supporting Information Fig. S7).

Comparison with DFT TS Geometries

Olsen et al.[12] listed O···H and C···H bond distances (r_{OH} and r_{CH}) for the DFT quartet TS structures, and the SAM1 UHF doublet results were compared to these (Fig. 7 and Supporting Information Fig. S8). In general, the SAM1 UHF TS bond distances showed moderate to good agreement with the DFT results: R^2 = 0.79 and MAD = 0.020 ± 0.011 Å for r_{OH} and R^2 = 0.62 and MAD = 0.015 ± 0.012 Å for r_{CH}. No obvious structural features were associated with the greatest deviations. Thus, SAM1 TS geometries can be used to estimate the absolute and relative DFT TS O···H bond distances and, to a lesser degree of accuracy, C···H bond distances. However, other SAM1 TS geometry aspects (e.g., bond and dihedral angles) were not as consistent with DFT results (Supporting Information Table S3).

TS Energies by SAM1 Reaction Path Calculation Using $OFeSCH_3$ (Proximal Ligand–SCH_3)

Reaction Path Calculation: Forward Direction, UHF

Direct SAM1 TS optimization of the quartet was problematic, making comparison with the results of Olsen et al.[12] difficult; so, we evaluated an alternative approach to estimate the activation energies: reaction path calculations, where the distance between the reacting atoms was incrementally reduced, with energy optimiza-

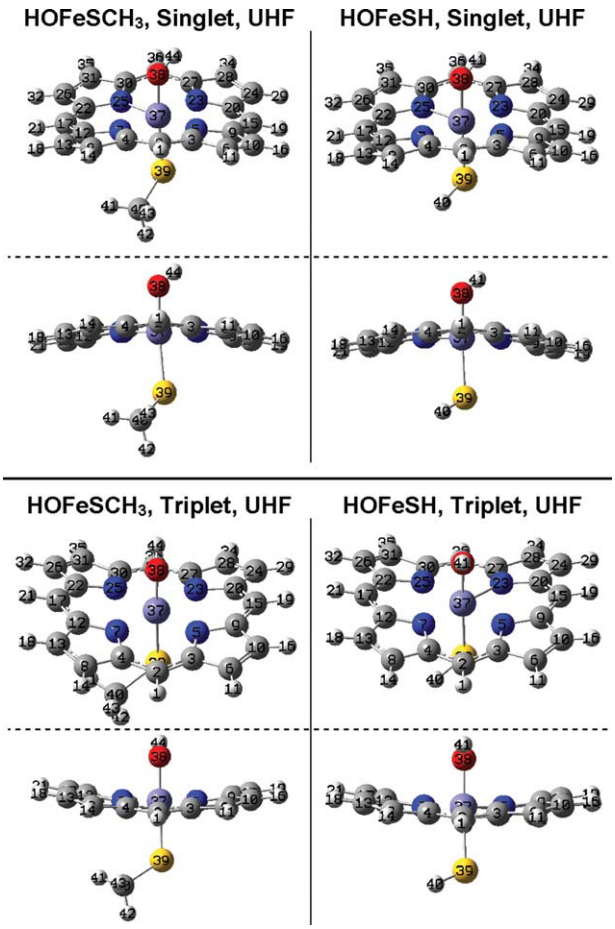

Figure 4. SAM1 UHF singlet geometries of iron-hydroxo species, $HOFeSCH_3$ and HOFeSH. The atom numbers define geometries listed in Table 2.

tion at each point. The transition-state structure enthalpy, H_f(TS), was obtained from the highest enthalpy structure of the reaction path, and the enthalpies of the reactants were subtracted to obtain the activation enthalpy. Calculating the reaction path in the forward direction (decreasing the O···H bond distance between the oxygen atom of the Cpd I, depicted as $(FeO)^{3+}$, and the hydrogen of the substrate; [eq. (1)]) often failed to generate the desired products (see Supporting Information Fig. S9 for a description of the problems). Calculations based on the reverse reaction, however, were found to more reliably produce the desired chemical species and were therefore studied instead [eq. (2)].

Forward reaction :

$$\text{Substrate} + (FeO)^{3+} \rightarrow \text{Substrate radical}^{\bullet} + (FeOH)^{3+} \quad (1)$$

Reverse reaction :

$$\text{Substrate radical}^{\bullet} + (FeOH)^{3+} \rightarrow \text{Substrate} + (FeO)^{3+} \quad (2)$$

The TS determined via the reverse direction is valid based on the principle of microscopic reversibility, which states that in a reversible reaction, the mechanism in one direction is exactly the reverse of the mechanism in the other direction.[65] Differences in reaction path calculations performed in the forward vs. the reverse direction have been documented and commented on previously by others.[64,66]

Reverse Reaction Path Calculation: UHF Doublet Spin State

The activation enthalpies were calculated by the RRP approach, using different SAM1 methodologies: UHF and CI. A representative reaction coordinate is depicted in Supporting Information Figure S10. For the RRP calculation, the starting species are the hydroxo-iron-porphine (HOFeSX) and the substrate radical, both of which were individually energy optimized before beginning the reaction path calculation. The RRP $\Delta H^{\ddagger}$ (UHF, doublet) correlated well with $\Delta H^{\ddagger}$ calculated via direct TS optimization, with $R^2 = 0.97$ (see Fig. 8), indicating that the RRP method can generally estimate the relative $\Delta H^{\ddagger}$. However, the slope of the regression line ($\Delta H^{\ddagger}_{pred} = 1.25 \cdot \Delta H^{\ddagger}_{RRP} - 15.62$) was 1.25, a substantial deviation from unity, with the RRP method overestimating the TS-optimized $\Delta H^{\ddagger}$, except for methane. In the regression, methane showed the largest residual; when methane is excluded from the regression analysis, the regression line is $1.13 \cdot \Delta H^{\ddagger}_{RRP} - 10.98$ ($R^2 = 0.96$), with a slope closer to unity. Thus, the $\Delta H^{\ddagger}$ determined via the RRP method was generally consistent with that calculated from optimized TS structures, both after offset.

A comparison of these SAM1 RRP $\Delta H^{\ddagger}$ (UHF, doublet) to the DFT activation energies ($\Delta E^{\ddagger}$) reported by Olsen et al.[12] is shown in Fig. 6 and Table 4 and Supporting Information Table S4. The starting spin state of the HOFeSX influenced the TS enthalpy of formation (H_f) and geometry, with HOFeSX previ-

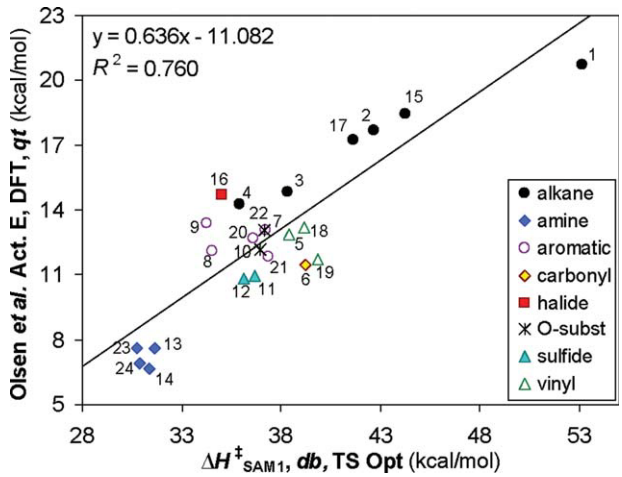

Figure 5. Correlation of DFT activation energy (using $OFeSCH_3$ from Olsen et al.[12]) with SAM1 UHF $\Delta H^{\ddagger}$. Here, the quartet spin state of Olsen et al.[12] is compared with the doublet SAM1 results. The number labels correspond to substrates listed in Table 3. The solid line represents the least-squares fit using all points. SAM1 UHF $\Delta H^{\ddagger}$ was calculated from the optimized TS structure. The legend indicates the type of substituent attached to the reactive carbon center.

Table 3. SAM1 UHF Doublet Enthalpy of Formation for the TS Structure [Substrate···H···$OFeSCH_3$], the Activation Enthalpy and Enthalpy for the Associated Reaction (Substrate-H + $OFeSCH_3$ → Substrate Radical + $HOFeSCH_3$), and Comparison with DFT Results of Olsen et al.[12]

		SAM1 enthalpies (kcal/mol), db					Olsen et al.[12] DFT activation energy[c]		SAM1 $\Delta H^{\ddagger}$ after offset[d]	Difference (SAM1 offset $\Delta H^{\ddagger}$ − Olsen)
#	Substrate	H_f(sub) RHF	H_f(rad) UHF	H_f(TS)[a] UHF	ΔH(rxn)	$\Delta H^{\ddagger}$[b](calc)	qt (kcal/mol)	Difference (SAM1 $\Delta H^{\ddagger}$ − Olsen)		
1	Methane	−16.20	29.69	116.97	51.85	53.12	20.72	32.40	28.40	7.68
2	Propane(1)	−25.82	9.22	96.88	40.99	42.65	17.66	24.99	17.93	0.27
3	Propane(2)	−25.82	0.33	92.57	32.10	38.34	14.82	23.52	13.62	−1.20
4	Isobutane	−30.31	−11.64	85.66	24.62	35.92	14.27	21.65	11.20	−3.07
5	Propene	5.21	30.39	123.65	31.13	38.39	12.88	25.51	13.67	0.78
6	Propionaldehyde	−47.61	−19.98	71.70	33.58	39.26	11.45	27.81	14.54	3.09
7	Toluene	9.68	34.58	126.97	30.85	37.24	13.05	24.19	12.52	−0.53
8	Ethylbenzene(1)	5.10	22.83	119.69	23.68	34.53	12.09	22.44	9.81	−2.28
9	*i*-Propylbenzene	1.31	13.19	115.64	17.84	34.28	13.34	20.94	9.56	−3.78
10	Dimethylether	−45.93	−15.25	71.10	36.63	36.98	12.17	24.81	12.26	0.09
11	Dimethylsulfide	−6.22	21.67	110.54	33.84	36.70	10.97	25.73	11.98	1.01
12	Me(Ph)sulfide	20.78	47.63	136.97	32.80	36.15	10.85	25.29	11.42	0.57
13	Dimethylamine	−5.32	17.91	106.38	29.19	31.65	7.62	24.03	6.93	−0.69
14	Trimethylamine	−4.37	18.82	107.05	29.15	31.37	6.67	24.71	6.65	−0.02
15	Fluoroethane(2)	−64.27	−27.70	60.07	42.52	44.29	18.45	25.84	19.57	1.12
16	Fluoroethane(1)	−64.27	−42.21	50.80	28.01	35.02	14.72	20.30	10.30	−4.43
17	Ethylbenzene(2)	5.10	39.62	126.76	40.48	41.61	17.26	24.35	16.89	−0.37
18	2-Fluoroprop-1-ene	−38.55	−11.88	80.68	32.62	39.18	13.19	25.99	14.46	1.26
19	Prop-1-en-2-ol	−38.78	−10.89	81.09	33.84	39.81	11.74	28.08	15.09	3.36
20	*p*-Xylene	−0.12	24.02	116.55	30.10	36.62	12.67	23.95	11.90	−0.77
21	*p*-Nitrotoluene	3.44	28.86	120.84	31.38	37.36	11.83	25.53	12.64	0.81
22	Methoxybenzene	−14.98	15.29	102.21	36.22	37.14	13.03	24.11	12.42	−0.61
23	*N*-Methylaniline	21.27	42.33	132.10	27.01	30.78	7.62	23.15	6.06	−1.57
24	*N*,*N*-Dimethylaniline	24.18	45.97	135.13	27.75	30.90	6.91	23.99	6.18	−0.73
		HOFe	OFe				Mean=	24.72	MAD=	1.67
	$OFeSCH_3$	86.00	80.05				SD=	2.47	SD=	1.78

Correlation of SAM1 $\Delta H^{\ddagger}$ with activation energy reported by Olsen et al.[12]: $R^2 = 0.760$. Without offset, −11.082 (±2.878) + 0.636 · $\Delta H^{\ddagger}_{SAM1}$ (±0.076); with offset, 4.640 (±1.036) + 0.636 · $\Delta H^{\ddagger}_{SAM1}$ (±0.076); () = standard error of the intercept or slope; residual standard error = 1.768.

[a] H_f(TS) obtained from the gradient-optimized TS structure; TS was verified by the presence of only one imaginary frequency and by IRC. For substrates methyl phenyl sulfide and ethylbenzene(2), TS determination was more difficult and required looser convergence criterion than the other substrates (i.e., the RMS gradient norm tolerance was set to 0.01, rather than 0.001).

[b] Activation enthalpies ($\Delta H^{\ddagger}$) were calculated by subtracting the heat of formation of the reactants ($OFeSCH_3$ and substrate) from the TS enthalpy.

[c] DFT energies determined at B3LYP/6–311++G(2d,2p)//B3LYP/6–31G(d) level, with ZPE at the B3LYP/6–31G(d)level included. For iron, double-ζ basis set of Schäfer et al.[67] enhanced with a p function with the exponent 0.134915. All energies are relative to the sum of the energies of the isolated substrate and the compound I model.

[d] Offset = Mean difference (SAM1 $\Delta H^{\ddagger}$ − DFT activation energy[12]).

ously energy optimized in the singlet state leading to results more consistent with DFT results than HOFeSX optimized in the triplet state; isopropylbenzene and *p*-nitrotoluene were the notable outliers when using the triplet-optimized HOFeSX (see Supporting Information Table S5 and Figs. S11 and S12). Thus, the singlet-optimized HOFeSX was used as the starting structure for the RRP calculations.

The RRP SAM1 UHF $\Delta H^{\ddagger}$ results for the doublet were all shifted upward relative to DFT ($\Delta E^{\ddagger}$), by an average of 29.9 ± 1.7 kcal/mol; however, when this value was subtracted, the SAM1 $\Delta H^{\ddagger}$ was in very good agreement with DFT $\Delta E^{\ddagger}$, with a MAD of 1.3 ± 1.0 kcal/mol (Table 4 and Fig. 6). Substrates with the largest [SAM1 − DFT] activation energy difference were fluoroethane(1) (Δ = −3.9 kcal/mol), methane (2.9 kcal/mol), propionaldehyde (2.9 kcal/mol), isopropylbenzene (−2.8 kcal/mol), prop-1-en-2-ol (2.1 kcal/mol), and isobutane (2.0 kcal/mol), with all other substrates showing an absolute difference of less than 1.8 kcal/mol, after offset. Interestingly, the RRP MAD was somewhat smaller than that using optimized TS structures (*vide supra*; Table 3; MAD = 1.7 ± 1.8 kcal/mol).

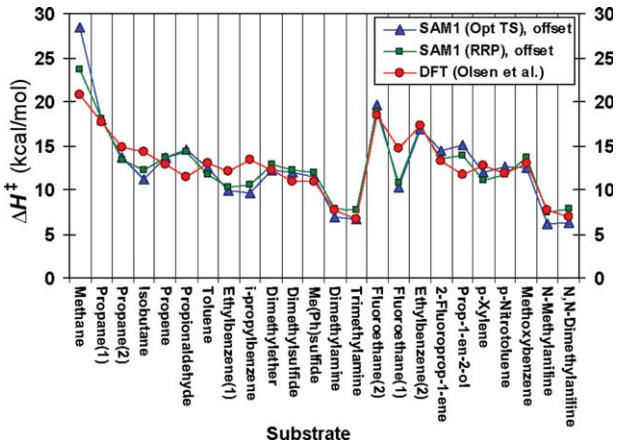

Figure 6. Comparison of DFT activation energies calculated by Olsen et al.[12] to activation enthalpies ($\Delta H^{\ddagger}$) calculated by SAM1 (UHF, doublet) reverse reaction path and by TS optimization methods. For ease of comparison, the SAM1 $\Delta H^{\ddagger}$ has been offset by the MAD (24.72 and 29.87 kcal/mol for the optimized TS and RRP methods, respectively) between DFT[12] activation energies and our SAM1 $\Delta H^{\ddagger}$ values. Here, for simplicity, the *y*-axis is labeled $\Delta H^{\ddagger}$, although the Olsen et al.[12] data are activation energies. [Color figure can be viewed in the online issue, which is available at wileyonlinelibrary.com.]

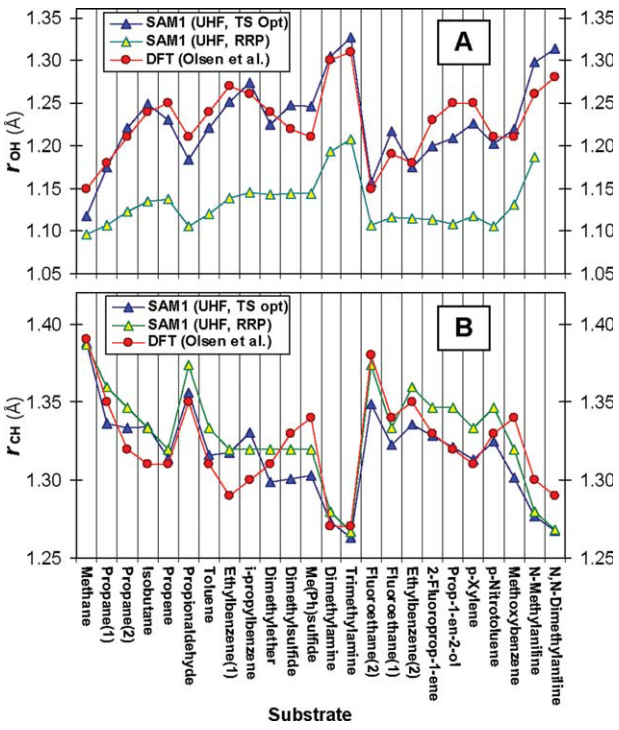

Figure 7. Comparison of the TS geometry calculated by DFT B3LYP (quartet; Olsen et al.[12]) and by SAM1 doublet UHF TS optimization and RRP approaches: bond distances for (A) O—H bond (r_{OH}) and (B) C—H bond (r_{CH}). Distances are in angstroms (Å). [Color figure can be viewed in the online issue, which is available at wileyonlinelibrary.com.]

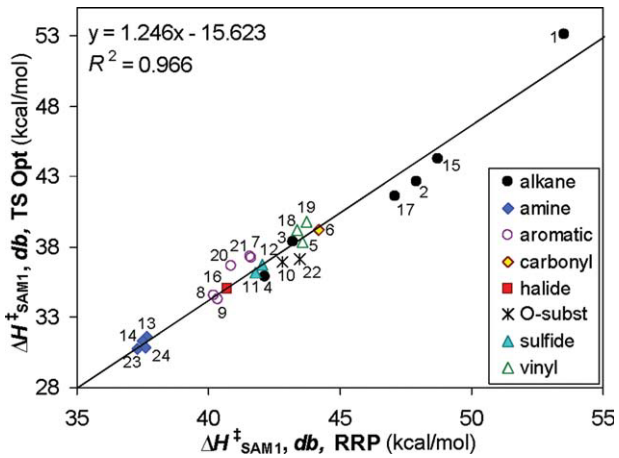

Figure 8. Comparison of SAM1 UHF activation enthalpy ($\Delta H^{\ddagger}$) calculated by TS optimization and by the reverse reaction path (RRP) approach for the doublet spin state. The number labels correspond to substrates listed in Table 3. The legend indicates the type of substituent attached to reactive carbon center. [Color figure can be viewed in the online issue, which is available at wileyonlinelibrary.com.]

Correlation of SAM1 UHF RRP $\Delta H^{\ddagger}$ and DFT activation energy[12] gave an R^2 value of 0.81, slightly higher than the corresponding correlation of 0.76 using SAM1-optimized TS H_fs.

Thus, overall, the UHF RRP approach yielded activation enthalpies slightly more consistent with DFT values than those from direct TS calculations, based on these 21 substrates.

RRP: UHF Quartet

For the quartet spin state, however, major issues were encountered using the UHF RRP approach, such as the fragmentation of the porphine ring and unusual behavior for all nitrogen-containing substrates, during the reaction (Supporting Information Fig. S13). The ether and thioether substrates also showed notable deviations from the DFT activation energy[12] (Supporting Information Fig. S14). Thus, the applicability of quartet UHF RRP is limited, and we were able to determine TS enthalpies for only 20 of the 24 positions (Supporting Information Fig. S14). Interestingly, however, the relative DFT activation energy[12] of the fluorine substrates, fluoroethane(1) and fluoroethane(2), is better predicted by using the quartet than the doublet spin state. Further details on the quartet RRP results are presented in the Supporting Information (Supporting Information Figs. S13 and S14).

RRP: CI Doublet Spin State

In an attempt to improve accuracy, we conducted CI calculations. Performing the CI reaction path calculations in the forward direction [eq. (1)], however, was problematic, resulting in convergence failures under all settings examined. Thus, we applied the RRP approach, using the same starting geometries for the reactants as was used in the UHF RRP calculations. Initial CI calculations were performed using OPEN(1,1), followed by OPEN(3,3) (see footnotes in the Tables and Supporting Information for details on computational settings). For the doublet,

Table 4. Comparison of SAM1 Activation Enthalpy (kcal/mol), Calculated Using Different Methods and the Reverse Reaction Path Approach, with the DFT Quartet Activation Energy Reported by Olsen et al.[12]

	SAM1 UHF RRP Doublet		SAM1 three CI-active MOs RRP							
			OPEN(1,1) doublet		OPEN(3,3) doublet		OPEN(1,1) quartet		OPEN(3,3) quartet	
Substrate no.	$\Delta H^{\ddagger}$ after offset[a]	Difference (SAM1 − DFT)	$\Delta H^{\ddagger}$ after offset[a]	Difference (SAM1 − DFT)	$\Delta H^{\ddagger}$ after offset[a]	Difference (SAM1 − DFT)	$\Delta H^{\ddagger}$ after offset[a]	Difference (SAM1 − DFT)	$\Delta H^{\ddagger}$ after offset[a]	Difference (SAM1 − DFT)
1	23.64	2.92	23.35	2.63	23.83	3.11	23.02	2.29	23.47	2.75
2	18.03	0.36	16.84	−0.83	17.37	−0.29	16.87	−0.79	16.87	−0.79
3	13.35	−1.47	12.81	−2.01	13.25	−1.56	12.88	−1.94	12.67	−2.15
4	12.27	−2.00	10.29	−3.97	10.04	−4.23	10.41	−3.86	10.09	−4.17
5	13.70	0.81	14.48	1.60	14.66	1.78	14.51	1.63	14.59	1.71
6	14.31	2.87	13.20	1.75	13.38	1.93	12.58	1.13	12.60	1.15
7	11.74	−1.31	15.25	2.20	15.40	2.35	15.23	2.18	15.67	2.62
8	10.31	−1.79	12.31	0.22	12.02	−0.07	12.30	0.21	12.28	0.18
9	10.49	−2.84	11.51	−1.83	10.98	−2.36	11.56	−1.78	11.27	−2.07
10	12.91	0.75	11.30	−0.86	11.04	−1.12	11.22	−0.94	10.98	−1.19
11	12.18	1.21	10.16	−0.81	9.90	−1.07	10.65	−0.32	10.30	−0.68
12	11.92	1.07	10.70	−0.15	10.22	−0.63	10.67	−0.18	10.50	−0.35
13	7.79	0.17	5.81	−1.81	5.33	−2.29	6.08	−1.54	5.72	−1.90
14	7.65	0.98	5.02	−1.65	5.11	−1.56	5.43	−1.24	5.67	−1.00
15	18.84	0.38	18.10	−0.35	18.32	−0.13	17.87	−0.58	17.93	−0.53
16	10.83	−3.89	8.71	−6.01	8.62	−6.10	8.60	−6.12	8.36	−6.36
17	17.20	−0.05	17.27	0.01	17.45	0.19	16.94	−0.32	16.94	−0.31
18	13.52	0.32	16.13	2.94	16.37	3.17	16.08	2.88	16.18	2.99
19	13.85	2.12	16.08	4.35	16.22	4.49	16.06	4.33	16.10	4.37
20	11.01	−1.65	14.97	2.30	15.05	2.39	15.34	2.67	15.44	2.77
21	11.70	−0.13	15.64	3.80	15.72	3.88	15.35	3.52	15.70	3.87
22	13.60	0.58	12.60	−0.42	12.36	−0.67	12.46	−0.57	12.26	−0.77
23	7.40	−0.23	6.79	−0.83	6.65	−0.98	6.88	−0.75	7.16	−0.47
24	7.74	0.83	6.65	−0.25	6.68	−0.23	6.99	0.08	7.23	0.32
	MAD=	1.28	MAD=	1.82	MAD=	1.94	MAD=	1.74	MAD=	1.90
	SD=	1.05	SD=	1.53	SD=	1.59	SD=	1.53	SD=	1.60
	R^2 =	0.808[b]	R^2 =	0.699[b]	R^2 =	0.696[b]	R^2 =	0.692[b]	R^2 =	0.665[b]
	HOFe[c]	OFe	HOFe[c]	OFe[d]	HOFe[c]	OFe[d]	HOFe[c]	OFe[d]	HOFe[c]	OFe[d]
H_f	86.00	80.05	86.00	108.84	86.00	108.84	86.00	129.62	86.00	129.62

See Supporting Information Tables S4, S6, S7, S8, and S9 for raw data. Reaction path calculation was started with optimized singlet $HOFeSCH_3$ geometry.

[a] $\Delta H^{\ddagger}$ after offset was determined as follows: (1) activation enthalpy ($\Delta H^{\ddagger}$) was calculated by subtracting the H_f of the reactants ($OFeSCH_3$ and substrate, individually optimized) from the TS enthalpy H_f(TS), taken from the highest point in the reaction path; (2) the offset is the mean of the pairwise differences between SAM1 $\Delta H^{\ddagger}$ and DFT[12]; (3) $\Delta H^{\ddagger}$ after offset is $\Delta H^{\ddagger}$ minus the offset.

[b] Correlation of SAM1 $\Delta H^{\ddagger}$ with DFT activation energy reported by Olsen et al.[12] See Supporting Information Tables S4, S6, S7, S8, and S9 for regression equations.

[c] HOFe is always singlet, UHF.

[d] H_f ($OFeSCH_3$) is 3CI, OPEN(3,3) energy-optimized enthalpy: 129.62 is the quartet, whereas 108.84 is the doublet.

the 3CI OPEN(1,1) RRP $\Delta H^{\ddagger}$ showed less agreement with DFT quartet results (MAD = 1.8 ± 1.5 kcal/mol; R^2 = 0.70) (Table 4 and Supporting Information Table S6), compared with UHF RRP (1.3 ± 1.0 kcal/mol, R^2 = 0.81; Table 4 and Supporting Information Fig. S15; *vide supra*), both after offset. With CI, the substrates with the largest [SAM1 − DFT] activation energy difference, after offset, were fluoroethane(1) (Δ = −6.0 kcal/mol), prop-1-en-2-ol (4.3 kcal/mol), isobutane (−4.0 kcal/mol), *p*-nitrotoluene (3.8 kcal/mol), 2-fluoroprop-1-ene (2.9 kcal/mol), and methane (2.6 kcal/mol), with all other substrates showing a difference of less than 2.4 kcal/mol. *p*-Nitrotoluene and 2-fluoroprop-1-ene showed poor agreement here with DFT, whereas using UHF, they showed excellent agreement.

Changing the CI settings to 3CI OPEN(3,3), for the doublet RRP, yielded marginally less agreement of $\Delta H^{\ddagger}$ with DFT quartet results[12] (MAD = 1.9 ± 1.6 kcal/mol; R^2 = 0.70; Table 4 and

Supporting Information Table S7 and Fig. S16), compared with 3CI OPEN(1,1) RRP (MAD = 1.8 ± 1.5 kcal/mol, R^2 = 0.70; Table 4 and Supporting Information Fig. S16; *vide supra*), both after offset. With 3CI OPEN(3,3), the substrates with the largest [SAM1 − DFT] activation energy difference, after offset, were identical to those calculated using 3CI OPEN(1,1): fluoroethane(1) (Δ = −6.1 kcal/mol), prop-1-en-2-ol (4.5 kcal/mol), isobutane (−4.2 kcal/mol), *p*-nitrotoluene (3.9 kcal/mol), 2-fluoroprop-1-ene (3.2 kcal/mol), and methane (3.1 kcal/mol), with all other substrates showing a difference of less than 2.4 kcal/mol. The standard deviation of the MAD using 3CI OPEN(3,3) was also marginally larger than that found using 3CI OPEN(1,1).

RRP: CI Quartet Spin State

The RRP approach using CI, for the quartet, successfully gave TS enthalpies for all 21 substrates (Supporting Information Table S8), in sharp contrast with UHF TS optimization and UHF RRP approaches for the quartet, which yielded only 11 and 20 TS enthalpies, respectively (Supporting Information Table S2 and Fig. S14). The CI OPEN(1,1) RRP quartet $\Delta H^{\ddagger}$, after offset, showed similar agreement with DFT quartet results (MAD = 1.7 ± 1.5 kcal/mol; R^2 = 0.69; Table 4 and Supporting Information Table S8) compared to the corresponding doublet RRP $\Delta H^{\ddagger}$ (MAD = 1.8 ± 1.5 kcal/mol; R^2 = 0.70; Table 4). The substrates with the largest [SAM1 − DFT] activation energy difference, after offset, were the same as for the doublet for the first five substrates: fluoroethane(1) (Δ = −6.1 kcal/mol), prop-1-en-2-ol (4.3 kcal/mol), isobutane (−3.9 kcal/mol), *p*-nitrotoluene (3.5 kcal/mol), 2-fluoroprop-1-ene (2.9 kcal/mol), and *p*-xylene (2.7 kcal/mol).

Changing the CI settings to 3CI OPEN(3,3), for the quartet RRP, yielded less agreement of $\Delta H^{\ddagger}$ with DFT quartet results[12] (MAD = 1.9 ± 1.6 kcal/mol; R^2 = 0.66; Table 4 and Supporting Information Table S9 and Fig. S16), compared with 3CI OPEN(1,1) RRP (MAD = 1.7 ± 1.5 kcal/mol, R^2 = 0.69; Table 4; *vide supra*), both after offset. With 3CI OPEN(3,3), the substrates with the largest [SAM1 − DFT] activation energy difference, after offset, were similar to those calculated using 3CI OPEN(1,1): fluoroethane(1) (Δ = −6.4 kcal/mol), prop-1-en-2-ol (4.4 kcal/mol), isobutane (−4.2 kcal/mol), *p*-nitrotoluene (3.9 kcal/mol), 2-fluoroprop-1-ene (3.0 kcal/mol), *p*-xylene (2.8 kcal/mol), methane (2.7 kcal/mol), and toluene (2.6 kcal/mol), with all other substrates showing a difference of less than 2.4 kcal/mol. The standard deviation of the MAD, using 3CI OPEN(3,3), was also marginally larger than that calculated using 3CI OPEN(1,1).

RRP Calculation Time

For the 21 substrates, the SAM1 UHF and 3CI OPEN(1,1) RRP calculation time averaged 9 and 15 min per substrate, respectively, in real (wall-clock) time on a desktop workstation (Supporting Information Table S10A). When the calculation times of a subset of these substrates were compared to those for the corresponding (forward reaction) "relaxed scan" DFT calculation in G03 using a compute cluster (see Computational Methods for a description of the workstation and compute cluster), the SAM1 UHF and 3CI RRP calculation times were, on average, 500 and 270 times faster, respectively (Supporting Information Table S10C).

RRP Geometry: Comparison with DFT TS Geometries

The O···H and C···H bond distances (r_{OH} and r_{CH}) calculated by the RRP approach (UHF, doublet) were compared to the DFT quartet results of Olsen et al.[12] (Fig. 7 and Supporting Information Table S11). For r_{OH}, the SAM1 RRP consistently underestimated the DFT results, with a mean difference of 0.09 ± 0.03 Å (R^2 = 0.60); however, for r_{CH}, the RRP approach approximated the DFT reasonably well, with MAD = 0.016 ± 0.008 Å (R^2 = 0.72), comparable to SAM1 TS optimization results (*vide supra*). Thus, the SAM1 RRP approach can be used to estimate absolute and relative DFT C···H bond distance, with nearly the same accuracy as the computationally more expensive SAM1 TS optimization. To estimate DFT r_{OH} using SAM1 RRP, if the r_{OH} [SAM1 − DFT] offset is added to the SAM1 values, the r_{OH} [SAM1 − DFT] MAD = 0.023 ± 0.013 Å, which is somewhat larger than the MAD of 0.020 ± 0.011 Å, when comparing SAM1-optimized and DFT TS structures.

RRP Calculation Summary.

Based on 21 substrates, our findings demonstrate that the RRP procedure, using SAM1, can be used to estimate hydrogen abstraction activation enthalpies to within 1.3 ± 1.0 kcal/mol (UHF) and 1.7 ± 1.5 kcal/mol [3CI OPEN(1,1)] of DFT B3LYP values[12] and can be of great utility because of its simplicity and speed, with an average TS determination taking less than 10 and 16 min per substrate for UHF and CI calculations, respectively: on average 500 and 270 times faster than those for the corresponding DFT calculations. For the TS O···H and C···H bond distances, the RRP method estimates r_{CH} to within 0.016 ± 0.008 Å (no offset) and r_{OH} to within 0.023 ± 0.013 Å (after offset) of DFT values.

TS Energies by SAM1 RRP Calculation for Another Set of Substrates and Using OFeSH (Proximal Ligand–SH)

Substrates Previously Studied by Shaik et al.[21]

Shaik et al.[21] calculated DFT TSs, in both the doublet and quartet spin states, of several substrates for hydrogen abstraction using OFeSH, allowing direct spin state comparison with the corresponding SAM1 results. Here, the proximal ligand was —SH (rather than $-SCH_3$ used by Olsen et al.[12]), and we, accordingly, used the same ligand for the SAM1 calculations. Because the ligand, as well as the basis set used by Shaik et al.,[21] is different from that used by Olsen et al.,[12] our SAM1 results and analyses are separately compared. In addition to energy values, complete coordinate data were generally provided by Shaik et al.,[21] facilitating comparison with SAM1 results. This second set of substrates is called substrate set 2.

RRP: UHF Doublet and Quartet $\Delta H^{\ddagger}$

Like the previous 21 substrates, the SAM1 UHF RRP approach for the doublet for this second set of substrates was rapid, with no optimization difficulties, and comparison of the resulting SAM1 activation enthalpies with Shaik et al.'s[21] DFT doublet activation energies again showed very good agreement (MAD = 1.3 ± 0.7 kcal/mol after offset; R^2 = 0.89) (Table 5 and Fig. 9). The substrates with the largest [SAM1 − DFT] activation energy difference, after offset, were ethylbenzene(1) (Δ = −2.2 kcal/mol), *trans*-methylphe-

Table 5. SAM1 UHF Doublet Activation Enthalpy, Calculated Using the Reverse Reaction Path Approach, vs. DFT Activation Energy Doublet Results of Shaik et al.[21]

#	Substrate	SAM1 enthalpies (kcal/mol), db H_f(sub) RHF	H_f(TS)[a] UHF	$\Delta H^{\ddagger}$ (calc)[b]	Shaik et al.,[21] db DFT $\Delta E^{\ddagger}$ + ZPE[c] (kcal/mol)	Difference (SAM1 $\Delta H^{\ddagger}$ − Shaik)	SAM1 $\Delta H^{\ddagger}$ after offset	Difference (SAM1 offset $\Delta H^{\ddagger}$ − Shaik)
1	Methane	−16.20	113.34	53.83	22.34	31.49	22.75	0.41
2	Ethane	−21.11	102.51	47.91	15.30	32.61	16.82	1.52
3*i*	Propane(2)	−25.82	93.69	43.79	13.85	29.94	12.71	−1.14
3*n*	Propane(1)	−25.82	98.13	48.23	15.19	33.04	17.15	1.96
4	Propene	5.21	124.82	43.90	12.82	31.08	12.81	−0.01
5	*trans*-MePhCyclopropane	35.31	157.35	46.32	13.13	33.19	15.24	2.11
6	*trans*-*i*-PrPhCyclopropane	26.31	144.74	42.72	12.27	30.45	11.64	−0.63
7	*N*,*N*-Dimethylaniline	24.18	136.85	36.96	4.99	31.97	5.88	0.89
8	Toluene	9.68	127.21	41.81	12.05	29.76	10.73	−1.32
9	Ethylbenzene(1)	5.10	121.17	40.35	11.47	28.88	9.27	−2.20
10	Camphor[d]	−55.40	65.69	45.37	15.88	29.49	14.29	−1.59
	HOFeSH[e]	82.24			Mean=	31.08	MAD=	1.25
	OFeSH[e]	75.71			SD=	1.50	SD=	0.72

Correlation of SAM1 $\Delta H^{\ddagger}$ with DFT activation energy reported by Shaik et al.[21]: R^2 = 0.890. Without offset, −25.175 (±4.572) + 0.868 · $\Delta H^{\ddagger}_{SAM1}$ (±0.102); with offset, 1.795 (±1.45) + 0.868 · $\Delta H^{\ddagger}_{SAM1}$ (±0.102); () = standard error of the intercept or slope; residual standard error = 1.447.

[a] H_f(TS) obtained from the highest point in the reaction path. Reaction path calculated starting with optimized singlet HOFeSH geometry.

[b] Activation enthalpies ($\Delta H^{\ddagger}$) were calculated by subtracting the heat of formation of the reactants (OFeSH and substrate, individually optimized) from the TS enthalpy.

[c] Geometry optimizations (without constraints) followed by analytical frequency calculations were performed in G03 with an LACVP basis set on iron and a 6–31G basis set on the rest of the atoms (basis set B1). Subsequent, single-point calculations were done on the optimized geometries in Jaguar 7.0 using a triple-ζ quality LACV3P+ basis set on iron and 6–311+G* on the rest of the atoms (basis set B2). All ZPE values are from UB3LYP/B1 frequency calculations. $\Delta E^{\ddagger}$ was calculated relative to separated reactants, ^{4,2}Cpd I + Alk-H.

[d] The hydrogen abstracted from camphor was based on that abstracted in Shaik et al.[21]

[e] H_f for energy-optimized singlet HOFeSH, doublet OFeSH, both UHF.

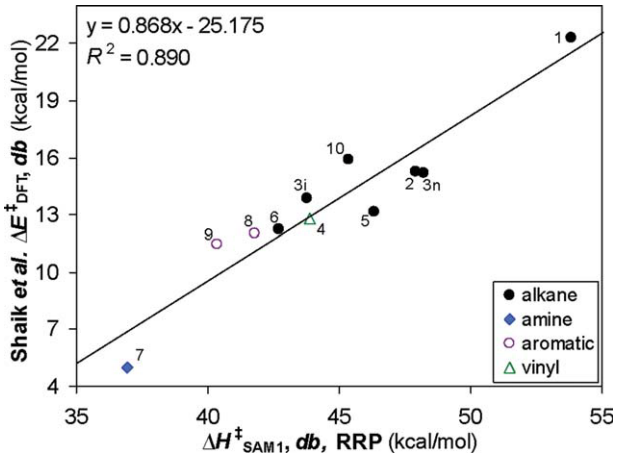

Figure 9. SAM1 UHF RRP doublet $\Delta H^{\ddagger}$ vs. doublet DFT activation energy calculated by Shaik et al.,[21] both using OFeSH. The number labels correspond to substrates listed in Table 5. The solid line represents the least-squares fit using all points. [Color figure can be viewed in the online issue, which is available at wileyonlinelibrary.com.]

nylcyclopropane (2.1 kcal/mol), and propane(1) (2.0 kcal/mol), with the other substrates showing a difference of less than 1.6 kcal/mol.

As before, the SAM1 UHF RRP approach for the quartet spin state was unsuccessful in determining the TS structure for the *N*-containing substrate *N*,*N*-dimethylaniline. This finding supports the previous results that indicated that the SAM1 UHF RRP approach is inadequate for calculating TS structures of substrates with a nitrogen α to the abstraction center, when the system is in the quartet spin state. See Supporting Information for data (Supporting Information Table S12 and Fig. S17).

RRP: CI Doublet and Quartet $\Delta H^{\ddagger}$, Three CI-Active MOs, OPEN(1,1)

CI calculations were performed using substrate set 2, initially with the same CI settings: three CI-active MOs, OPEN(1,1). As observed with substrate set 1, SAM1 CI doublet $\Delta H^{\ddagger}$ showed very good agreement with the DFT doublet results of Shaik et al.[21] (MAD = 1.2 ± 1.0 kcal/mol after offset; R^2 = 0.85; Table 6 and Supporting Information Table S13) and comparable to the SAM1 UHF doublet $\Delta H^{\ddagger}$ MAD = 1.3 ± 0.7 kcal/mol, R^2

Table 6. Comparison of SAM1 Activation Enthalpy (kcal/mol), Calculated Using Different Methods and the Reverse Reaction Path Approach, with the DFT Doublet and Quartet Activation Energy Reported by Shaik et al.[21]

	SAM1 three CI-active MOs								SAM1 four CI-Active MOs			
	OPEN(1,1)				OPEN(3,3)				OPEN(1,1)			
	Doublet		Quartet		Doublet		Quartet		Doublet		Quartet	
No.	$\Delta H^{\ddagger}$ after offset[a]	Difference (SAM1 − DFT)	$\Delta H^{\ddagger}$ after offset[a]	Difference (SAM1 − DFT)	$\Delta H^{\ddagger}$ after offset[a]	Difference (SAM1 − DFT)	$\Delta H^{\ddagger}$ after offset[a]	Difference (SAM1 − DFT)	$\Delta H^{\ddagger}$ after offset[a]	Difference (SAM1 − DFT)	$\Delta H^{\ddagger}$ after offset[a]	Difference (SAM1 − DFT)
1	22.43	0.09	22.96	0.05	22.91	0.57	23.23	0.32	22.68	0.34	23.10	0.19
2	15.58	0.28	16.48	−0.93	15.70	0.40	16.50	−0.91	15.60	0.30	16.23	−1.18
3*i*	11.85	−2.00	12.78	−3.02	11.75	−2.10	12.55	−3.25	11.65	−2.20	12.47	−3.33
3*n*	15.91	0.72	16.79	−0.69	16.03	0.84	16.77	−0.71	15.89	0.70	16.60	−0.88
4	13.55	0.73	13.98	1.03	13.65	0.83	14.39	1.44	13.65	0.83	14.33	1.38
5	14.78	1.65	15.89	1.36	14.86	1.73	15.76	1.23	14.84	1.71	15.80	1.27
6	11.20	−1.07	12.22	−1.24	10.86	−1.41	11.84	−1.62	10.64	−1.63	11.88	−1.58
7	5.58	0.59	6.87	1.33	5.06	0.07	7.05	1.51	5.32	0.33	7.01	1.47
8	14.30	2.25	15.19	2.76	14.43	2.38	15.35	2.92	14.55	2.50	15.57	3.14
9	11.64	0.17	12.88	0.33	11.59	0.12	12.73	0.18	12.12	0.65	13.24	0.69
10	12.47	−3.41	13.54	−0.97	12.46	−3.42	13.40	−1.11	12.35	−3.53	13.33	−1.18
	MAD=	1.18	MAD=	1.25	MAD=	1.26	MAD=	1.38	MAD=	1.34	MAD=	1.48
	SD=	1.04	SD=	0.91	SD=	1.06	SD=	0.96	SD=	1.07	SD=	0.95
	R^2 =	0.852[b]	R^2 =	0.860[b]	R^2 =	0.849[b]	R^2 =	0.834[b]	R^2 =	0.831[b]	R^2 =	0.818[b]
	HOFe[c]	OFe[c]	HOFe[c]	OFe[d]	HOFe[c]	OFe[c]	HOFe[c]	OFe[d]	HOFe	OFe	HOFe	OFe
H_f	82.24	105.32	82.24	124.87	82.24	104.21	82.24	124.87	82.24	96.24	82.24	132.00

See Supporting Information Tables S13, S14, S16, S17, and S18 for raw data. Reaction path calculation was started with optimized singlet HOFeSH geometry.

[a] $\Delta H^{\ddagger}$ after offset was determined as follows: (1) activation enthalpy ($\Delta H^{\ddagger}$) was calculated by subtracting the H_f of the reactants (OFeSH and substrate) from the TS enthalpy H_f(TS), taken from the highest point in the reaction path; (2) the offset is the mean of the pairwise differences between SAM1 $\Delta H^{\ddagger}$ and DFT; (3) $\Delta H^{\ddagger}$ after offset is $\Delta H^{\ddagger}$ minus the offset.

[b] Correlation of SAM1 $\Delta H^{\ddagger}$ with DFT activation energy reported by Shaik et al.[21] See Supporting Information Tables S13, S14, S16, S17, and S18 for regression equations.

[c] H_f for energy-optimized singlet HOFeSH using UHF; for doublet OFeSH using 3CI OPEN(1,1), where the three CI-active MOs are LUMO, HOMO, and HOMO-1. OPEN(1,1) optimization was only successful for doublet OFeSH. Quartet OFeSH, quartet $OFeSCH_3$, and doublet $OFeSCH_3$ all failed to converge.

[d] H_f for energy-optimized quartet OFeSH using 3CI OPEN(3,3), where the three CI-active MOs are LUMO, HOMO, and HOMO-1.

= 0.89; Table 5; *vide supra*). For this set, however, the spin state was the same for each method, allowing for direct comparison. The substrates with the largest [SAM1 − DFT] activation energy difference, after offset, differed from those calculated using SAM1 UHF: camphor (Δ = −3.4 kcal/mol), toluene (2.2 kcal/mol), and propane(2) (−2.0 kcal/mol); the other substrates showed a difference of less than 1.7 kcal/mol.

A major advantage of CI is for the quartet spin state, which was problematic using UHF methods. Using CI, the RRP approach was successful in estimating quartet TS enthalpies for each substrate. Comparison of the SAM1 quartet CI RRP $\Delta H^{\ddagger}$ with DFT quartet $\Delta E^{\ddagger}$, by Shaik et al.,[21] revealed very good agreement (MAD = 1.2 ± 0.9 kcal/mol after offset; R^2 = 0.86; Table 6 and Supporting Information Table S14). The [SAM1 − DFT] deviations were generally similar to those observed for the doublet, with the largest deviations occurring with propane(2) (−3.0 kcal/mol) and toluene (2.8 kcal/mol), and all other substrates showed a difference of less than 1.4 kcal/mol. Camphor was distinctive in that it displayed a [SAM1 − DFT] deviation of only 1.0 kcal/mol for the quartet, although it showed the largest deviation among the doublet substrates (−3.4 kcal/mol).

Although the correlation of SAM1 $\Delta H^{\ddagger}$ with DFT activation energies was somewhat higher for the substrate set of Shaik et al.[21] than for that of Olsen et al.,[12] this result is likely due to the smaller number and variety of substrates in the set studied by Shaik et al.,[21] which included 10 substrates (11 positions), whereas the set examined by Olsen et al.[12] included 21 substrates (24 positions). Based on our classification scheme, the former set of substrates comprises four structural classes (alkane, amine, aromatic, and vinyl), whereas the latter set comprises eight classes (alkane, amine, aromatic, carbonyl, halide, *O*-substituted, sulfide, and vinyl).

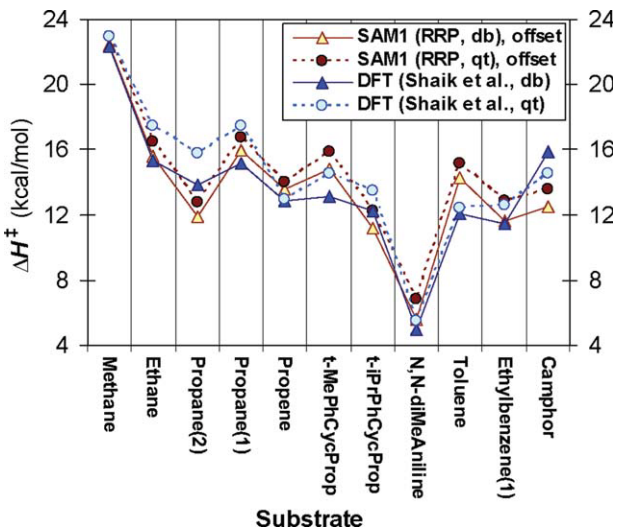

Figure 10. SAM1 3CI OPEN(1,1) activation enthalpies obtained from reverse reaction path calculations, plotted with the DFT activation energies calculated by Shaik et al.[21] All values are in kcal/mol. The SAM1 values were offset by the MAD from Shaik et al.'s[21] energies to allow for easier comparison. [Color figure can be viewed in the online issue, which is available at wileyonlinelibrary.com.]

Figure 10 summarizes the activation energies calculated by SAM1 3CI OPEN(1,1) and by DFT[21] and shows that, within each model chemistry, the quartet spin system gave higher values than that of the doublet for all substrates except camphor. With DFT,[21] an inversion of the quartet–doublet activation energy for camphor was observed, whereas with SAM1, the energy hierarchy remained consistent with the other substrates. The SAM1 3CI OPEN(1,1) doublet–quartet activation enthalpy difference was 9.10 ± 0.3 kcal/mol (0.9 ± 0.3 kcal/mol, after both offset), whereas the DFT doublet–quartet activation enthalpy difference was 0.9 ± 1.1 kcal/mol (1.2 ± 0.8 kcal/mol excluding camphor), indicating that hydrogen abstraction activation energies of the quartet can be reasonably estimated from the doublet energies and relative ordering should parallel each other between the spin states.

For the RRP method, $\Delta H^{\ddagger}$ is calculated by subtracting the H_fs of the substrate and OFeSX (each individually optimized) from the H_f of highest point on the reaction coordinate. We compared this way of calculating $\Delta H^{\ddagger}$ to that calculated by subtracting the H_f corresponding to the enthalpy of the system of reactants (usually the lowest point in the reaction coordinate), rather than the individually optimized reactants; the results of the reactant system subtraction revealed a higher MAD with DFT $\Delta H^{\ddagger}$ (Supporting Information Table S15). Thus, the use of individually optimized reactants for the RRP approach yields results more consistent with those of DFT than subtraction of the energy of the system of reactants taken from the reaction coordinate.

Effect of Different CI Settings on RRP $\Delta H^{\ddagger}$: Three CI-Active MOs, OPEN(3,3)

As mentioned above, SAM1 calculations using three CI-active MOs with OPEN(3,3) were found to optimize all four OFeSX species (HS^- and CH_3S^- ligands with doublet and quartet spin multiplicities) without convergence failure. Thus, these settings [3CI OPEN(3,3)] were applied to the RRP method of determining activation enthalpies of the doublet and quartet.

For the doublet, comparison of the SAM1 CI [3CI OPEN(3,3)] RRP $\Delta H^{\ddagger}$ with DFT doublet $\Delta E^{\ddagger}$, by Shaik et al.,[21] revealed very good agreement (MAD = 1.3 ± 1.1 kcal/mol after offset; R^2 = 0.85) (Table 6 and Supporting Information Table S16); however, the deviation was marginally larger than that observed for [3CI OPEN(1,1)] RRP (MAD = 1.2 ± 1.0 kcal/mol, R^2 = 0.85; Table 6). The deviations exhibited the exact same pattern as 3CI OPEN(1,1), with identical substrates showing the greatest deviation from DFT: camphor, toluene, and propane(2). The 3CI OPEN(3,3) settings lowered the H_f by a near uniform constant of 1.0 ± 0.3 kcal/mol (Table 7) relative to 3CI OPEN(1,1).

For the quartet, comparison of the SAM1 quartet CI [3CI OPEN(3,3)] RRP $\Delta H^{\ddagger}$ with DFT quartet $\Delta E^{\ddagger}$, by Shaik et al.,[21] was similar to that for the doublet: the quartet showed very good agreement (MAD = 1.4 ± 1.0 kcal/mol after offset; R^2 = 0.83) (Table 6 and Supporting Information Table S17); however, the deviation was slightly larger than that observed for [3CI OPEN(1,1)] RRP (MAD = 1.2 ± 0.9 kcal/mol, R^2 = 0.86; *vide supra*). The deviations exhibited the exact same pattern as 3CI OPEN(1,1), with identical substrates showing the greatest devia-

Table 7. SAM1 CI [Four MOs,[a] OPEN(1,1)] Enthalpy Results, for the Doublet and Quartet, Calculated Using the Reverse Reaction Path Approach.

		H_f(TS)[b] (kcal/mol) 4-CI MO,[a] OPEN(1,1)		H_f(TS) difference[c] (3CI – 4CI), kcal/mol		H_f(TS) difference, 3-CI OPEN(1,1) – OPEN(3,3)[d]	
#	Substrate	Doublet	Quartet	Doublet	Quartet	Doublet	Quartet
1	Methane	137.69	167.63	2.04	0.35	−1.45	4.70
2	Ethane	125.70	155.85	2.27	0.75	−1.09	4.95
3*i*	Propane(2)	117.05	147.39	2.49	0.80	−0.87	5.20
3*n*	Propane(1)	121.29	151.52	2.31	0.68	−1.09	4.99
4	Propene	150.08	180.27	2.19	0.15	−1.07	4.56
5	*trans*-MePhCyclopropane	181.37	211.84	2.23	0.59	−1.05	5.10
6	*trans*-*i*-PrPhCyclopropane	168.17	198.92	2.85	0.84	−0.63	5.35
7	*N*,*N*-Dimethylaniline	160.71	191.92	2.55	0.36	−0.44	4.79
8	Toluene	155.45	185.99	2.04	0.12	−1.10	4.82
9	Ethylbenzene(1)	148.44	179.08	1.81	0.13	−0.91	5.11
10	Camphor	88.17	118.66	2.41	0.71	−0.96	5.11
			Mean=	2.29	0.50	−0.97	4.97
			SD=	0.28	0.28	0.27	0.24

R^2 = 0.831 and 0.818 for correlation with DFT[21] for the doublet and quartet four CI-active OPEN(1,1), respectively. For the regression results, for the doublet, without offset, −29.643 (±6.52) + 0.89 · $H^{\ddagger}_{SAM1}$ (±0.134); with offset, 1.49 (±1.895) + 0.89 · $H^{\ddagger}_{SAM1}$ (±0.134); () = standard error of the intercept or slope; residual standard error = 1.791. For the quartet, without offset, −27.905 (±6.7) + 0.981 · $H^{\ddagger}_{SAM1}$ (±0.154); with offset, 0.278 (±2.313) + 0.981 · $H^{\ddagger}_{SAM1}$ (±0.154); residual standard error = 1.918.

[a]Four CI-active MOs: LUMO+1, LUMO, HOMO, and HOMO-1.

[b]H_f(TS) obtained from the highest point in the reaction path. Reaction path calculated starting with optimized singlet HOFeSH geometry.

[c]H_f(TS) difference was calculated by subtracting the four CI-active OPEN(1,1) H_f(TS) from the three CI-active OPEN(1,1) H_f(TS) (Supporting Information Tables S13 and S14).

[d]H_f(TS) difference was calculated by subtracting the three CI-active OPEN(3,3) H_f(TS) from the three CI-active OPEN(1,1) H_f(TS).

tion from DFT: propane(2) and toluene, and all other substrates showed a difference of less than 1.7 kcal/mol. The 3CI OPEN(3,3) settings lowered the H_f by a near uniform constant of 5.0 ± 0.2 kcal/mol (Table 7) relative to 3CI OPEN(1,1).

Effect of Different CI Settings on RRP $\Delta H^{\ddagger}$: Four CI-Active MOs, OPEN(1,1) and Others

The effect of using different CI calculation parameters and settings was explored. Increasing the number of CI-active MOs from 3 to 4 (adding the LUMO+1 MO), using the RRP approach for substrate set 2, while holding the other settings identical, slightly decreased in a nearly uniform extent the H_f(TS) for all substrates: 2.3 ± 0.3 and 0.5 ± 0.3 kcal/mol for the doublet and quartet, respectively (Table 7). The use of 4CI did not show an improvement of the correlation (or MAD) with DFT results over the other CI methods [3CI OPEN(1,1) or 3CI OPEN(3,3)]: 4CI OPEN(1,1) RRP $\Delta H^{\ddagger}$ vs. DFT $\Delta E^{\ddagger}$ gave, for the doublet, MAD = 1.3 ± 1.1 kcal/mol after offset and R^2 = 0.83; for the quartet, MAD = 1.5 ± 1.0 kcal/mol after offset and R^2 = 0.82 (Supporting Information Fig. S18 and Table S18). Thus, based on these substrates, 3CI OPEN(1,1) showed slightly better agreement with DFT than 3CI OPEN(3,3) or 4CI OPEN(1,1) (Table 6).

We evaluated other CI settings, e.g., 4CI OPEN(3,4) and 5CI OPEN(3,5), using both ligands (CH_3S^- and HS^-) and spin states (doublet and quartet); all of these calculations resulted in convergence failure, except for 4CI OPEN(3,4), doublet, for the HS^- ligand.

Summary of Prediction of Relative DFT $\Delta H^{\ddagger}$ Using the Different SAM1 RRP Methods

In summary, as shown in Table 8, for the doublet spin state, the relative DFT $\Delta E^{\ddagger}$ was best predicted using the SAM1 UHF RRP method, rather than the SAM1 CI methods. For the quartet, however, both the UHF and CI SAM1 RRP methods demonstrated inconsistencies in predicting the relative DFT $\Delta E^{\ddagger}$. For the CI calculation methods, 3CI OPEN(1,1) gave activation energies closer to the DFT results than 3CI OPEN(3,3) or 4CI OPEN(1,1), based on the substrates examined. In general, the DFT doublet and quartet activation energies were similar for each substrate, and the relative doublet activation energies can be used to estimate relative quartet activation energies.

RRP: Effect of Step Size on $\Delta H^{\ddagger}$

The use of smaller incremental steps (0.00018 Å) in the RRP approach on the SAM1 $\Delta H^{\ddagger}$ did not improve the correspondence with DFT values for 3CI OPEN(1,1) calculations (cf. Table 6 and Supporting Information Table S19). For the quartet, the use of the

Table 8. Prediction of Relative DFT $\Delta H^{\ddagger}$ (kcal/mol) Using the Different SAM1 RRP Methods

$\Delta H^{\ddagger}$, DFT (Shaik et al.[21])				$\Delta H^{\ddagger}$, SAM1 RRP (UHF), offset			
Doublet		Quartet		Doublet		Quartet	
Methane	22.34[a]	Methane	22.91[a]	Methane	22.75[a]	*t*-*i*-PrPhCycloPr	19.28[a]
Camphor	15.88[c]	Propane(1)	17.48[b]	Propane(1)	17.15[b]	Methane	18.24[b]
Ethane	15.30[c]	Ethane	17.41[b]	Ethane	16.82[b]	Propane(1)	15.37[c]
Propane(1)	15.19[c]	Propane(2)	15.80[c]	*t*-MePhCycloPr	15.24[c]	Ethane	15.19[c]
Propane(2)	13.85[d]	*t*-MePhCycloPr	14.53[c]	Camphor	14.29[c]	Ethylbenzene(1)	15.08[c]
t-MePhCycloPr	13.13[d]	Camphor	14.51[c]	Propene	12.81[d]	Propene	14.86[c]
Propene	12.82[d]	*t*-*i*-PrPhCycloPr	13.46[d]	Propane(2)	12.71[d]	*t*-MePhCycloPr	14.46[c]
t-*i*-PrPhCycloPr	12.27[d]	Propene	12.95[d]	*t*-*i*-PrPhCycloPr	11.64[e]	Camphor	14.30[c]
Toluene	12.05[d]	Ethylbenzene(1)	12.55[d]	Toluene	10.73[e]	Propane(2)	14.29[c]
Ethylbenzene(1)	11.47[e]	Toluene	12.43[d]	Ethylbenzene(1)	9.27[e]	Toluene	12.97[d]
N,*N*-DiMeAniline	4.99[f]	*N*,*N*-DiMeAniline	5.54[f]	*N*,*N*-DiMeAniline	5.88[f]	*N*,*N*-DiMeAniline	ND[a]
$\Delta H^{\ddagger}$, SAM1 RRP (3CI OPEN(1,1)), offset				$\Delta H^{\ddagger}$, SAM1 RRP (4CI OPEN(1,1)), offset			
Doublet		Quartet		Doublet		Quartet	
Methane	22.43[a]	Methane	22.96[a]	Methane	22.68[a]	Methane	23.10[a]
Propane(1)	15.91[c]	Propane(1)	16.79[b]	Propane(1)	15.89[c]	Propane(1)	16.60[b]
Ethane	15.58[c]	Ethane	16.48[b]	Ethane	15.60[c]	Ethane	16.23[b]
t-MePhCycloPr	14.78[c]	*t*-MePhCycloPr	15.89[c]	*t*-MePhCycloPr	14.84[c]	*t*-MePhCycloPr	15.80[c]
Toluene	14.30[c]	Toluene	15.19[c]	Toluene	14.55[c]	Toluene	15.57[c]
Propene	13.55[d]	Propene	13.98[d]	Propene	13.65[d]	Propene	14.33[c]
Camphor	12.47[d]	Camphor	13.54[d]	Camphor	12.35[d]	Camphor	13.33[d]
Propane(2)	11.85[e]	Ethylbenzene(1)	12.88[d]	Ethylbenzene(1)	12.12[d]	Ethylbenzene(1)	13.24[d]
Ethylbenzene(1)	11.64[e]	Propane(2)	12.78[d]	Propane(2)	11.65[e]	Propane(2)	12.47[d]
t-*i*-PrPhCycloPr	11.20[e]	*t*-*i*-PrPhCycloPr	12.22[d]	*t*-*i*-PrPhCycloPr	10.64[e]	*t*-*i*-PrPhCycloPr	11.88[e]
N,*N*-DiMeAniline	5.58[f]	*N*,*N*-DiMeAniline	6.87[f]	*N*,*N*-DiMeAniline	5.32[f]	*N*,*N*-DiMeAniline	7.01[f]

ND= Not determinable
Values (kcal/mol)
[a]> 19
[b][16–19]
[c][14–16]
[d][12–14]
[e][9–12]
[f]< 9

smaller step size increased the MAD marginally from 1.25 ± 0.91 to 1.32 ± 0.90 kcal/mol. Thus, the RRP of 75 steps over 2–1 Å (i.e., step size 0.0133 Å) is sufficient to produce good results.

TS Geometries by SAM1 RRP Calculation for Substrate Set 2 and Using OFeSH (Proximal Ligand–SH)

SAM1 UHF TS Geometries by RRP: Comparison with DFT

Shaik et al.[21] provided atomic coordinates for the DFT TS structures, allowing direct comparison with the SAM1 TS geometries calculated by the RRP approach.

For the breaking C···H bond in the TS, the SAM1 UHF RRP bond length (r_{CH}) exhibited a pattern similar to that observed with DFT, when methane and camphor are excluded, with the UHF doublet bond length greater than DFT by 0.060 ± 0.019 Å (excluding methane and camphor) and R^2 = 0.69 (excluding methane and camphor) (Fig. 11 and Supporting Information Fig. S19). For the forming O···H bond, again excluding methane and camphor, the doublet RRP UHF pattern was similar to DFT, except that the bond length was shorter by 0.138 ± 0.037 Å (R^2 = 0.81).

For the quartet, the SAM1 UHF RRP TS r_{CH} pattern was similar to that observed with DFT, excluding *N*,*N*-dimethylaniline (which could not be calculated) (see Fig. 11); however, the UHF quartet bond length was shorter than DFT by 0.253 ± 0.030 Å (R^2 = 0.82; Supporting Information Fig. S19), again excluding *N*,*N*-dimethylaniline. For r_{OH}, the UHF quartet bond length was longer than DFT by 0.050 ± 0.025 Å (R^2 = 0.78; Supporting Information Fig. S19), without *N*,*N*-dimethylaniline.

Comparison of other geometry measurements showed little correlation between SAM1 UHF RRP and DFT results, except for a_{FeOH}, which demonstrated an R^2 of 0.77 and 0.80 for dou-

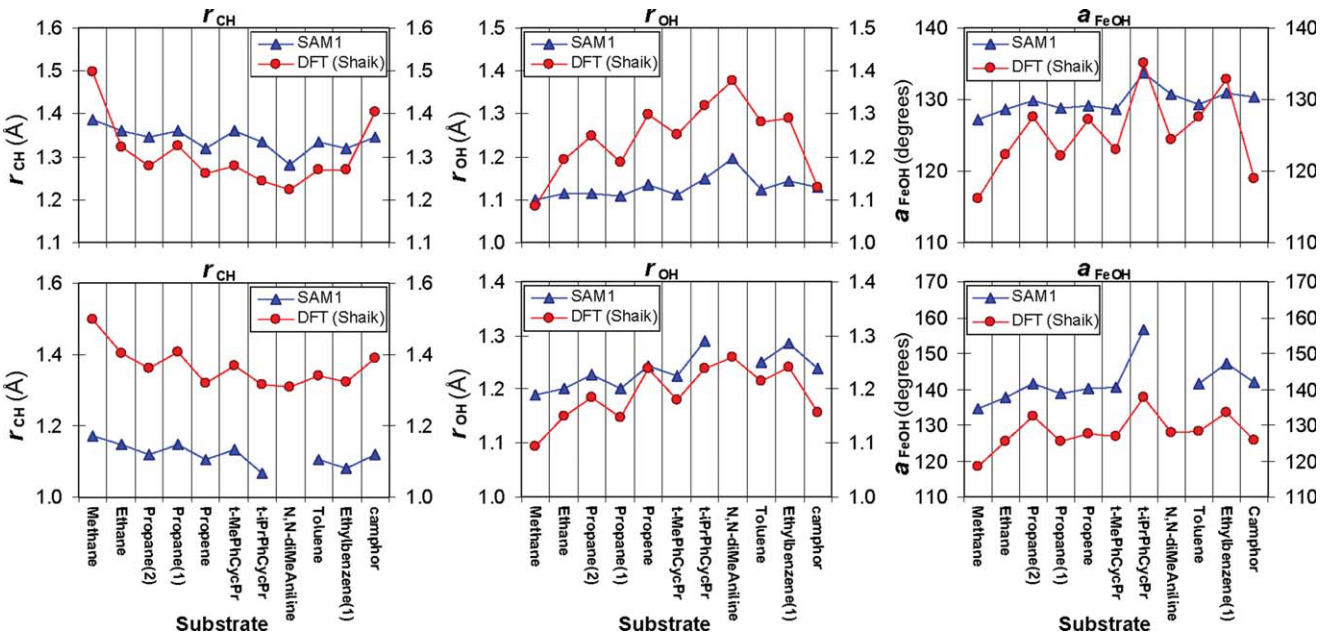

Figure 11. Comparison of the TS geometry calculated by SAM1 UHF RRP and DFT B3LYP (Shaik et al.[21]) for doublet (top row) and quartet (bottom row) spin states, respectively. Distances are in angstroms (Å). [Color figure can be viewed in the online issue, which is available at wileyonlinelibrary.com.]

blet and quartet, respectively (Fig. 11 and Supporting Information Fig. S19).

Thus, the SAM1 UHF RRP method could be used to estimate the bond lengths, r_{OH} and r_{CH}, as well as the bond angle, a_{FeOH}, in the TS, although additional substrates should be examined to better understand the basis for the anomalous behavior of camphor.

SAM1 CI Transition-State Geometries by RRP: Comparison with DFT

For the doublet 3CI OPEN(1,1) TS via RRP, r_{CH}, r_{OH}, and a_{FeOH} were very close or nearly identical to the UHF values (cf. Figs. 11 and 12). However, for the quartet 3CI OPEN(1,1) TS via RRP, r_{CH}, r_{OH}, and a_{FeOH} differed with the UHF RRP val-

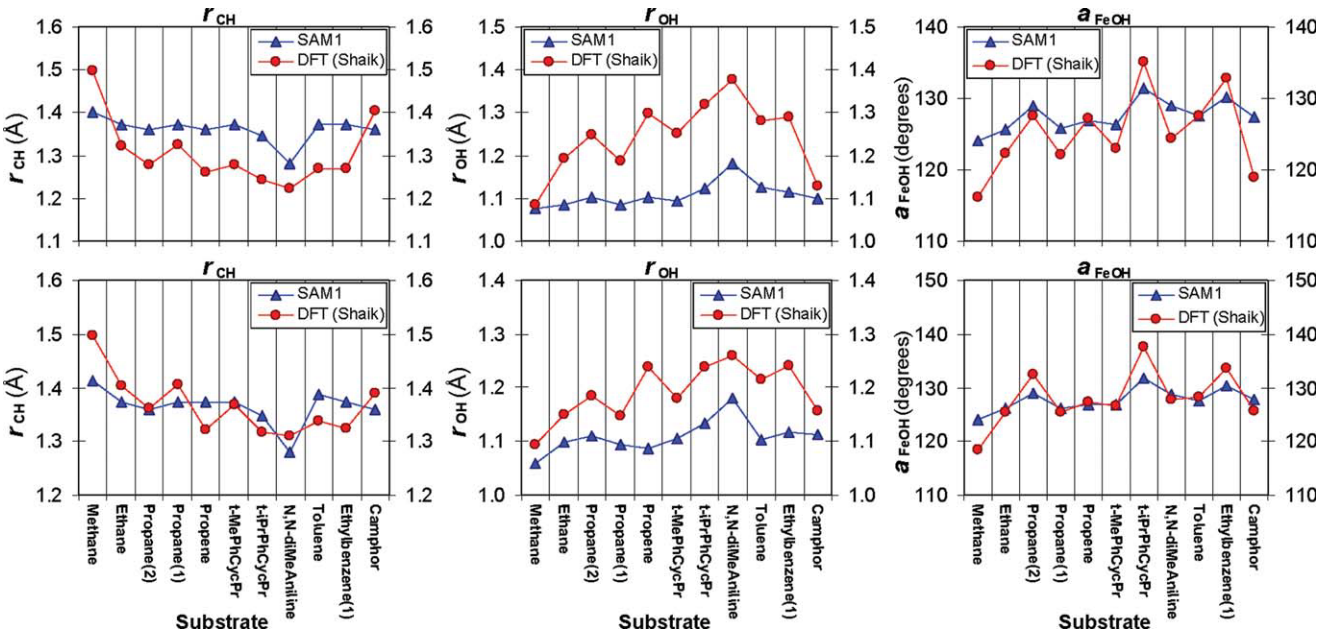

Figure 12. Comparison of the TS geometry calculated by SAM1 CI [three active MOs, OPEN(1,1)] RRP and DFT B3LYP (Shaik et al.[21]) for doublet (top row) and quartet (bottom row) spin states, respectively. Distances are in angstroms (Å). [Color figure can be viewed in the online issue, which is available at wileyonlinelibrary.com.]

ues, with the 3CI OPEN(1,1) geometry closer to the DFT for r_{CH} and a_{FeOH}, but farther for r_{OH}.

Correlation of SAM1 3CI RRP geometries with DFT values[21] revealed high correlation for a_{FeOH}, with an R^2 of 0.76 and 0.92 for doublet and quartet, respectively (Fig. 12 and Supporting Information Fig. S20), with the next highest correlation for r_{OH}, which showed an R^2 of 0.64 for the doublet (Supporting Information Fig. S20).

The SAM1 TS structures determined by UHF RRP and by CI RRP were generally similar for several geometry measurements (e.g., bond lengths for the doublet, Supporting Information Fig. S21A), although some differences were observed (e.g., bond angles and dihedral angles), particularly for the quartet. These similarities and differences are shown in Supporting Information Figures S21 and S22.

To summarize the SAM1 RRP TS geometry results, based on these substrates, 3CI OPEN(1,1) and UHF methodologies can be used to estimate DFT a_{FeOH} with good to excellent agreement, whereas the UHF methodology can estimate quartet DFT r_{CH} and r_{OH} with good agreement.

Ability to Use SAM1 TS Geometry as Starting Point for DFT TS Optimization

Direct Input of SAM1 TS Geometry for DFT TS Optimization

Because SAM1 calculations can be performed rapidly, we explored the use of SAM1 TS geometries as a starting point for DFT TS optimization. These calculations revealed that the use of SAM1 TS geometries as the initial structures for DFT TS optimizations yielded valid TS structures nearly every time, as verified by the presence of only one imaginary frequency. SAM1 TS geometries obtained via TS optimization and RRP (UHF and CI, for both doublet and quartet) could all be used. Furthermore, these DFT TS structures showed energies very similar to, or slightly lower than, those obtained by Shaik et al.[21] (Supporting Information Table S21), with the largest difference in TS energy 1.7 kcal/mol for propene. However, the DFT TS optimizations of SAM1 TSs were often more computationally expensive than the entire DFT job involving a reaction coordinate and TS optimization. Thus, the use of SAM1 TS geometries was not clearly advantageous, from a computational cost perspective.

Use of Key SAM1 TS Substrate-OFeSX Atomic Coordinates to Guide DFT TS Optimization

As the direct use of SAM1 TS structures did not reduce computation time, we investigated a DFT/SAM1 "hybrid" approach in an attempt to do so: this involved manually combining the DFT geometry-optimized OFeSH structure with the substrate geometry (and its relative orientation to OFeSH) taken from a SAM1 TS, i.e., key TS bond distances (O—H and C—H), angles (Fe—O—H, O—H—C), and dihedral angles (H—O—S—H and Fe—O—C—X) were taken from the SAM1 TS, and applied to the DFT OFeSH geometry, where X refers to any atom adjacent to the carbon from which the hydrogen is abstracted. DFT TS optimizations using this method showed a significant decrease in calculation time when compared with direct DFT optimization of a SAM1 TS (Supporting Information Table S21). Of the substrates examined, the DFT TS optimizations using the DFT/SAM1 hybrid method were, on average, 21% more rapid than determination of the TS entirely via DFT. Our studies suggest that SAM1 TS structures can be used to decrease the DFT TS calculation times, by taking the SAM1 substrate geometry and its orientation relative to the iron-oxo complex, rather than the entire SAM1 TS.

Conclusions

The SAM1 RRP approach, using iron-hydroxo-porphine, can be used to rapidly estimate DFT activation enthalpies and certain important geometry measurements. Thus, it can be applied to estimate the intrinsic hydroxylation rates and regioselectivity of substrates by the active oxygenating species within CYP enzymes, with computational times considerably shorter than those of DFT-only calculations. These data may assist in the evaluation of new drug candidates and extant chemicals for their potential to undergo bioactivation or detoxication by CYP enzymes and thus provide insights into the efficient selection of drug candidates and assessment of chemical risk.

Acknowledgments

The authors thank Prof. Anthony K. Rappé for helpful discussions as well as Dr. John Millam and Prof. Daniel Liotard.

References

1. Brown, C. M.; Reisfeld, B.; Mayeno, A. N. Drug Metab Rev 2008, 40, 1.
2. Parkinson, A. In Casarett and Doull's Toxicology: The Basic Science of Poisons; Klaassen, C. D., Ed.; McGraw-Hill: New York, 2008; pp. 161–304.
3. Guengerich, F. P. Chem Res Toxicol 2008, 21, 70.
4. Klopman, G.; Tu, M.; Fan, B. T. Theor Chem Acc 1999, 102, 33.
5. Jones, J. P.; Mysinger, M.; Korzekwa, K. R. Drug Metab Dispos 2002, 30, 7.
6. Borodina, Y.; Sadym, A.; Filimonov, D.; Blinova, V.; Dmitriev, A.; Poroikov, V. J Chem Inf Comput Sci 2003, 43, 1636.
7. Balakin, K. V.; Ekins, S.; Bugrim, A.; Ivanenkov, Y. A.; Korolev, D.; Nikolsky, Y. V.; Skorenko, A. V.; Ivashchenko, A. A.; Savchuk, N. P.; Nikolskaya, T. Drug Metab Dispos 2004, 32, 1183.
8. Mekenyan, O. G.; Dimitrov, S. D.; Pavlov, T. S.; Veith, G. D. Curr Pharm Des 2004, 10, 1273.
9. Cruciani, G.; Carosati, E.; De Boeck, B.; Ethirajulu, K.; Mackie, C.; Howe, T.; Vianello, R. J Med Chem 2005, 48, 6970.
10. Testa, B.; Balmat, A. L.; Long, A.; Judson, P. Chem Biodivers 2005, 2, 872.
11. Ekins, S.; Andreyev, S.; Ryabov, A.; Kirillov, E.; Rakhmatulin, E. A.; Bugrim, A.; Nikolskaya, T. Expert Opin Drug Metab Toxicol 2005, 1, 303.
12. Olsen, L.; Rydberg, P.; Rod, T. H.; Ryde, U. J Med Chem 2006, 49, 6489.
13. Crivori, P.; Poggesi, I. Eur J Med Chem 2006, 41, 795.
14. de Groot, M. J. Drug Discov Today 2006, 11, 601.
15. Afzelius, L.; Arnby, C. H.; Broo, A.; Carlsson, L.; Isaksson, C.; Jurva, U.; Kjellander, B.; Kolmodin, K.; Nilsson, K.; Raubacher, F.; Weidolf, L. Drug Metab Rev 2007, 39, 61.
16. Sheridan, R. P.; Korzekwa, K. R.; Torres, R. A.; Walker, M. J. J Med Chem 2007, 50, 3173.

17. Jolivette, L. J.; Ekins, S. In Advances in Clinical Chemistry, Vol. 43; Makowski, G., Ed.; Academic Press: San Diego, 2007; pp. 131–176.
18. Jung, J.; Kim, N. D.; Kim, S. Y.; Choi, I.; Cho, K. H.; Oh, W. S.; Kim, D. N.; No, K. T. J Chem Inf Model 2008, 48, 1074.
19. Madden, J. C.; Cronin, M. T. Expert Opin Drug Metab Toxicol 2006, 2, 545.
20. Oh, W. S.; Kim, D. N.; Jung, J.; Cho, K. H.; No, K. T. J Chem Inf Model 2008, 48, 591.
21. Shaik, S.; Kumar, D.; de Visser, S. P. J Am Chem Soc 2008, 130, 10128.
22. Czodrowski, P.; Kriegl, J. M.; Scheuerer, S.; Fox, T. Expert Opin Drug Metab 2009, 5, 15.
23. Zheng, M. Y.; Luo, X. M.; Shen, Q. C.; Wang, Y.; Du, Y.; Zhu, W. L.; Jiang, H. L. Bioinformatics 2009, 25, 1251.
24. Rydberg, P.; Vasanthanathan, P.; Oostenbrink, C.; Olsen, L. ChemMedChem 2009, 4, 2070.
25. Smith, J.; Stein, V. Comput Biol Chem 2009, 33, 149.
26. Hennemann, M.; Friedl, A.; Lobell, M.; Keldenich, J.; Hillisch, A.; Clark, T.; Goller, A. H. ChemMedChem 2009, 4, 657.
27. Kim, D. N.; Cho, K. H.; Oh, W. S.; Lee, C. J.; Lee, S. K.; Jung, J.; No, K. T. J Chem Inf Model 2009, 49, 1643.
28. Sun, H.; Scott, D. O. Chem Biol Drug Des 2010, 75, 3.
29. Coon, M. J. Biochem Biophys Res Commun 2003, 312, 163.
30. Danielson, P. B. Curr Drug Metab 2002, 3, 561.
31. Atkins, W. M. Annu Rev Pharmacol Toxicol 2005, 45, 291.
32. Atkins, W. M. Expert Opin Drug Metab Toxicol 2006, 2, 573.
33. Hlavica, P.; Lewis, D. F. V. Eur J Biochem 2001, 268, 4817.
34. Sligar, S. G.; Denisov, I. G. Drug Metab Rev 2007, 39, 567.
35. Research Collaboratory for Structural Biology (RCSB). Protein Data Bank. http://www.pdb.org.
36. Coon, M. J. Annu Rev Pharmacol Toxicol 2005, 45, 1.
37. Newcomb, M.; Hollenberg, P. F.; Coon, M. J. Arch Biochem Biophys 2003, 409, 72.
38. Newcomb, M.; Chandrasena, R. E. P. Biochem Biophys Res Commun 2005, 338, 394.
39. Meunier, B.; De Visser, S. P.; Shaik, S. Chem Rev 2004, 104, 3947.
40. Shaik, S.; Kumar, D.; de Visser, S. P.; Altun, A.; Thiel, W. Chem Rev 2005, 105, 2279.
41. Shaik, S.; Hirao, H.; Kumar, D. Nat Prod Rep 2007, 24, 533.
42. Guengerich, F. P. Chem Res Toxicol 2001, 14, 611.
43. de Groot, M. J.; Havenith, R. W. A.; Vinkers, H. M.; Zwaans, R.; Vermeulen, N. P. E.; van Lenthe, J. H. J Comput-Aided Mol Des 1998, 12, 183.
44. Oda, A.; Yamaotsu, N.; Hirono, S. J Comput Chem 2005, 26, 818.
45. Schoneboom, J. C.; Neese, F.; Thiel, W. J Am Chem Soc 2005, 127, 5840.
46. Korzekwa, K. R.; Jones, J. P.; Gillette, J. R. J Am Chem Soc 1990, 112, 7042.
47. Jones, J. P.; Korzekwa, K. R. Methods Enzymol 1996, 272, 326.
48. Park, J. Y.; Harris, D. J Med Chem 2003, 46, 1645.
49. Mayeno, A. N.; Robinson, J. L.; Yang, R. S. H.; Reisfeld, B. J Chem Inf Model 2009, 49, 1692.
50. Dewar, M. J. S.; Jie, C. X.; Yu, J. G. Tetrahedron 1993, 49, 5003.
51. Holder, A. J. Abstr Pap Am Chem Soc 1994, 207, 22.
52. Holder, A. J.; Dennington, R. D., II; Jie, C. Tetrahedron 1994, 50, 627.
53. Anslyn, E. V.; Dougherty, D. A. Modern Physical Organic Chemistry; University Science Books: Sausalito, CA, 2006.
54. Frisch, M. J.; Trucks, G. W.; Schlegel, H. B.; Scuseria, G. E.; Robb, M. A.; Cheeseman, J. R.; Montgomery, J. A., Jr.; Vreven, T.; Kudin, K. N.; Burant, J. C.; Millam, J. M.; Iyengar, S. S.; Tomasi, J.; Barone, V.; Mennucci, B.; Cossi, M.; Scalmani, G.; Rega, N.; Petersson, G. A.; Nakatsuji, H.; Hada, M.; Ehara, M.; Toyota, K.; Fukuda, R.; Hasegawa, J.; Ishida, M.; Nakajima, T.; Honda, Y.; Kitao, O.; Nakai, H.; Klene, M.; Li, X.; Knox, J. E.; Hratchian, H. P.; Cross, J. B.; Bakken, V.; Adamo, C.; Jaramillo, J.; Gomperts, R.; Stratmann, R. E.; Yazyev, O.; Austin, A. J.; Cammi, R.; Pomelli, C.; Ochterski, J. W.; Ayala, P. Y.; Morokuma, K.; Voth, G. A.; Salvador, P.; Dannenberg, J. J.; Zakrzewski, V. G.; Dapprich, S.; Daniels, A. D.; Strain, M. C.; Farkas, O.; Malick, D. K.; Rabuck, A. D.; Raghavachari, K.; Foresman, J. B.; Ortiz, J. V.; Cui, Q.; Baboul, A. G.; Clifford, S.; Cioslowski, J.; Stefanov, B. B.; Liu, G.; Liashenko, A.; Piskorz, P.; Komaromi, I.; Martin, R. L.; Fox, D. J.; Keith, T.; Al-Laham, M. A.; Peng, C. Y.; Nanayakkara, A.; Challacombe, M.; Gill, P. M. W.; Johnson, B.; Chen, W.; Wong, M. W.; Gonzalez, C.; Pople, J. A. Gaussian 03; Gaussian, Inc.: Wallingford, CT, 2004.
55. Dennington, R., II; Keith, T.; Millam, J. GaussView 4; Semichem, Inc.: Shawnee Mission, KS, 2007.
56. Dewar, M. J. S.; Holder, A. J.; Dennington, R. D., II; Liotard, D. A.; Truhlar, D. G.; Keith, T. A.; Millam, J. M.; Harris, C. D. AMPAC 9 User Manual; Semichem, Inc.: Shawnee Mission, KS, 2008.
57. Bathelt, C. M.; Ridder, L.; Mulholland, A. J.; Harvey, J. N. Org Biomol Chem 2004, 2, 2998.
58. Hirao, H.; Kumar, D.; Thiel, W.; Shaik, S. J Am Chem Soc 2005, 127, 13007.
59. Ogliaro, F.; Harris, N.; Cohen, S.; Filatov, M.; de Visser, S. P.; Shaik, S. J Am Chem Soc 2000, 122, 8977.
60. Göller, A. H.; Clark, T. J Mol Struct-Theochem 2001, 541, 263.
61. Groves, J. T. J Chem Educ 1985, 62, 928.
62. Shaik, S.; Cohen, S.; de Visser, S. P.; Sharma, P. K.; Kumar, D.; Kozuch, S.; Ogliaro, F.; Danovich, D. Eur J Inorg Chem 2004, 207.
63. Sastri, C. V.; Lee, J.; Oh, K.; Lee, Y. J.; Lee, J.; Jackson, T. A.; Ray, K.; Hirao, H.; Shin, W.; Halfen, J. A.; Kim, J.; Que, L.; Shaik, S.; Nam, W. Proc Natl Acad Sci USA 2007, 104, 19181.
64. McIver, J. W.; Komornicki, A. J Am Chem Soc 1972, 94, 2625.
65. Smith, M. B.; March, J. March's Advanced Organic Chemistry: Reactions, Mechanisms, and Structure; Wiley-Interscience: Hoboken, NJ, 2007.
66. Müller, K. Angew Chem Int Ed Engl 1980, 19, 1.
67. Schäfer, A.; Horn, H.; Ahlrichs, R. J Chem Phys 1992, 97, 2571.